

DISSERTATION DER FAKULTÄT FÜR BIOLOGIE DER
LUDWIG-MAXIMILIANS-UNIVERSITÄT MÜNCHEN

**INFLUENCE OF DEVELOPMENT, TONOTOPY AND HEARING
DISORDERS ON THE BIOPHYSICAL PROPERTIES OF
AUDITORY BRAINSTEM NEURONS**

Christina Berger

Diese Dissertation wurde angefertigt unter der Leitung von Dr. Felix Felmy an der Fakultät für Biologie der Ludwig-Maximilians-Universität München.

Erstgutachter: Prof. Dr. Felix Felmy

Zweitgutachter: Prof. Dr. Benedikt Grothe

Tag der Abgabe: 27. April 2016

Tag der mündlichen Prüfung: 07. Februar 2017

ERKLÄRUNG

Ich versichere hiermit an Eides statt, dass meine Dissertation selbständig und ohne unerlaubte Hilfsmittel angefertigt worden ist. Die vorliegende Dissertation wurde weder ganz, noch teilweise bei einer anderen Prüfungskommission vorgelegt. Ich habe noch zu keinem früheren Zeitpunkt versucht, eine Dissertation einzureichen oder an einer Doktorprüfung teilzunehmen.

München, den 08.05.2017

Christina Berger

CONTENTS

ABSTRACT	9
ZUSAMMENFASSUNG	11
I. INTRODUCTION	13
1. The mammalian auditory pathway	13
The peripheral auditory system	13
The central auditory system	15
ITD and ILD coding in mammals	17
2. Early development and refinement of auditory brainstem circuits	19
Early development of the auditory brainstem	19
Synaptic refinement in auditory brainstem nuclei	20
Development of intrinsic cell properties	23
3. Mouse Models for Hearing disorders	25
The mouse as a model for hearing loss	26
Genes and pathways involved in hearing disorders	27
The Diminuendo mouse	30
The Claudin-14-knockout mouse	32
4. Aims	34
II. MATERIAL AND METHODS	36
1. Animals	36
2. Slice preparation	36
3. Electrophysiology	37
4. Immunohistochemistry and confocal microscopy	38
5. Image and data analysis	39

III. RESULTS	41
1. Development of GABAergic and glycinergic inputs to the LSO in mice and gerbils.	41
Miniature IPSCs before and after hearing onset	42
Evoked IPSCs in prehearing mice and gerbils	45
2. Characterization of cells and inputs in the adult mouse LSO along the tonotopic axis	48
Characterization of passive and active properties of LSO neurons	49
Synaptic transmission in the mature LSO	53
3. Consequences of two deafness-related mutations for a large central auditory synapse	57
Morphology	59
Passive properties	61
Active properties and firing behavior	64
Miniature EPSCs	69
Evoked EPSCs	71
AMPA and NMDA currents	76
IV. DISCUSSION	80
1. Development of GABAergic and glycinergic inputs	81
Development and species-specific differences	81
No evidence for co-release of GABA and glycine	83
2. Characterization of Cells types and Inputs in the LSO	86
Two different cell types in the LSO	86
Excitatory and inhibitory inputs	88
Little evidence for tonotopy-dependent adaptations in the mouse LSO	88
3. Consequences of deafness-related Mutations	90
Comparability of both mutants	91
Maturation of synaptic morphology	92

Altered synaptic transmission in the Diminuendo mutant _____	93
Immature AMPAR and NMDAR mediated currents in Diminuendo mice _____	96
Alteration of specific intrinsic properties by the miR-96 mutation _____	97
Summary and outlook _____	99
LITERATURE _____	101
LIST OF ABBREVIATIONS _____	111
LIST OF FIGURES _____	113
DANKSAGUNG _____	115

ABSTRACT

The development and function of the auditory system requires a complex interplay of genetically encoded programs, spontaneous activity and sensory experience. The basic projection patterns between auditory brainstem nuclei develop during fetal life. The topographic representation of frequencies established in the cochlea, the so-called tonotopy, is present at almost all stages of the auditory system. The development of auditory brainstem circuits involves a refinement of these projections and a maturation of cellular and synaptic properties. This work studies different aspects of development and function of the binaural auditory system with respect to species-specific differences, the influence of tonotopy on certain cellular and synaptic properties and the consequences of two deafness-related mutations.

The first project examines the early postnatal development of the inhibitory projection from the medial nucleus of the trapezoid body (MNTB) to the lateral superior olive (LSO), a tonotopically arranged nucleus involved in binaural sound localization. The detection of small differences in sound intensity between the two ears requires a temporally and spatially precise convergence of the binaural excitatory and inhibitory inputs. During development, the inhibitory projection undergoes a shift from predominantly GABAergic to glycinergic transmission. In this project, this switch in transmitter type was comparatively studied in pre-hearing mice and gerbils by analyzing miniature and evoked inhibitory postsynaptic currents (IPSCs). In both animals, an increase in miniature IPSC amplitude and frequency was shown, as well as acceleration of the decay kinetics. However, the application of a GABA_A antagonist did not provide evidence for a simultaneous release of both transmitters. Possible explanations for the GABAergic component observed in evoked IPSCs involve a spillover of GABA from other synapses and that other projections besides the MNTB provide additional inhibitory input to the LSO.

The second study addresses the question whether the tonotopic arrangement of the LSO of adult mice is reflected in adaptations on the cellular and synaptic level. The characterization of different intrinsic properties of LSO neurons revealed the existence of two distinct

neuronal populations that display differences regarding their firing type and input resistance. Cells that exhibited an onset firing behavior probably showed a mediolateral gradient in their input resistance. The analysis of evoked and miniature IPSCs in mice could not provide clear evidence for position-dependent adaptations.

A third set of experiments studies the consequences of two mutations associated with deafness in mice and humans. The *Diminuendo* mutation is the first known mutation of a microRNA related to hearing disorders. MicroRNA-96 regulates the expression of numerous genes involved in inner ear development and mutations are accompanied by defects of the peripheral auditory system, but its function in the central auditory system has not been investigated yet. This study examines the consequences of this mutation for a large central auditory synapse, the calyx of Held, and its postsynaptic partners in the MNTB. Since there is no conditional knockout available yet, another deaf mouse model, the Claudin-14 knockout mouse, served as control. In this mouse, the defect is exclusively peripheral. The comparison of both mutants allows to distinguish between peripheral and central defects. The study demonstrated that neither the mutation of miR-96 nor deafness had a significant effect on the passive membrane properties of MNTB neurons. However, *Diminuendo* mice showed a higher proportion of cells displaying an immature firing behavior. Studying the presynaptic morphology provided further hints for a developmental arrest. Calyces in *Diminuendo* mice did not possess the donut-like structures characteristic for adult animals but appeared rather immature. On a functional level, excitatory postsynaptic currents in the *Diminuendo* mutant displayed a stronger depression, suggesting a faster depletion of the vesicle pool, which is also in accordance with the idea of a developmental arrest. This hypothesis is further supported by the analysis of NMDA and AMPA receptor mediated currents, which display immature properties regarding their amplitude and kinetics. In summary, this study provides evidence that mutations of miR-96 result in a developmental arrest of several pre- and postsynaptic properties in the brainstem, similar to its function in the peripheral auditory system, while the influence of deafness on the calyx of Held-MNTB synapse is rather small.

ZUSAMMENFASSUNG

Die korrekte Entwicklung und Funktion des auditorischen Systems erfordert ein komplexes Zusammenspiel aus genetisch vorgegebenen Programmen, spontaner neuronaler Aktivität und sensorischem Input. Die grundlegenden Verbindungen zwischen den Nuclei des auditorischen Hirnstamms entwickeln sich frühzeitig während der Embryonalentwicklung. Die bereits in Cochlea etablierte tonotopische Organisation, also die räumlich geordnete Repräsentation von Frequenzen, wird dabei auf vielen Stufen des zentralen auditorischen Systems beibehalten. Die weitere Entwicklung geht einher mit der Verfeinerung bestehender Projektionen und einer Reifung der zellulären und synaptischen Eigenschaften. Diese Arbeit befasst sich mit verschiedenen Aspekten der Entwicklung und Funktion des binauralen auditorischen Systems in Hinblick auf Spezies-spezifische Unterschiede, den Einfluss von Tonotopie auf zelluläre und synaptische Eigenschaften und die Auswirkungen von zwei mit Taubheit assoziierten Mutationen.

In einem ersten Projekt wurde die frühe postnatale Entwicklung der inhibitorischen Projektion vom medialen Nucleus des Trapezkörpers (MNTB) zur lateralen superioren Olive (LSO) betrachtet. Die LSO ist ein tonotopisch organisierter Nucleus, dessen Hauptaufgabe in der Lokalisation einer Schallquelle anhand von Lautstärkenunterschieden an beiden Ohren besteht, was die präzise räumliche und zeitliche Konvergenz des binauralen Inputs erfordert. Während der Entwicklung durchläuft die inhibitorische Projektion einen Wechsel des vorherrschenden Transmittertyps von GABA zu Glycin, der in dieser Arbeit komparativ in Mäusen und Gerbils durch die Analyse von Miniatur- und evozierten postsynaptischen Strömen (IPSCs) untersucht wurde. In beiden Tieren zeigte sich eine entwicklungsabhängige beschleunigte Kinetik und eine Zunahme in Frequenz und Amplitude der Minis, allerdings fanden sich keine Hinweise auf die simultane Freisetzung beider Transmitter. Mögliche Erklärungen für die GABAerge Komponente, die sich in den evozierten IPSCs zeigte, beinhalten Spillover und die Existenz einer zusätzlichen Quelle inhibitorischen Inputs außerhalb des MNTB.

Das zweite Projekt befasste sich mit der Frage, inwieweit sich die tonotopische Organisation der LSO adulter Mäuse in Anpassungen auf zellulärer und synaptischer Ebene widerspiegelt. Die Studie zeigte die Existenz zweier verschiedener Populationen von Neuronen, die sich vor allem durch ihr Feuerverhalten und ihren Eingangswiderstand unterschieden. Neuronen, die durch ein Onset-Aktionspotential charakterisiert waren, wiesen einen mediolateralen Gradienten bezüglich ihres Eingangswiderstands auf. Die Analyse der postsynaptischen Ströme lieferte keine klaren Anhaltspunkte für Tonotopie-spezifische Anpassungen.

In einer dritten Studie wurden die Auswirkungen zweier Mutationen untersucht, die auch im Menschen mit Taubheit assoziiert sind. *Diminuendo* stellt die erste bekannte Mutation einer microRNA dar, die mit Taubheit in Verbindung steht. MicroRNA-96 reguliert die Expression zahlreicher in die Entwicklung des Innenohrs involvierter Gene und Mutationen gehen mit schweren Defekten des peripheren auditorischen Systems einher, aber ihre Auswirkungen auf das zentrale auditorische System wurden bisher nicht erforscht. Diese Arbeit untersucht die Konsequenzen der Mutation für die Entwicklung einer großen auditorischen Synapse, der Held'schen Calyx und ihrer postsynaptischen Partner im MNTB. Dazu wurde die *Diminuendo*-Maus mit einer anderen Mutante, der Claudin-14-knockout-Maus verglichen, in der die Mutation ausschließlich das periphere auditorische System betrifft. Der Vergleich beider Mäuse ermöglicht die Trennung zwischen peripheren und zentralen Defekten. Die Studie konnte zeigen, dass weder Taubheit im Allgemeinen noch die Mutation von miR-96 signifikante Auswirkungen auf die passiven Membraneigenschaften haben, allerdings wiesen *Diminuendo*-Mäuse einen höheren Anteil an Neuronen mit unreifem Feuerverhalten auf. Morphologisch waren die präsynaptischen Donut-artigen Strukturen, die charakteristisch für die adulte Calyx sind, weniger ausgeprägt. Funktionell zeigten diese Synapsen eine stärkere Depression der postsynaptischen Ströme, was auf eine schnellere Erschöpfung des Vesikel-Pools hindeutet. Auch die AMPA- und NMDA-Rezeptor vermittelten Ströme wiesen unreife Charakteristika auf. Insgesamt kann man also feststellen, dass die Mutation von miR-96, ähnlich wie im peripheren auditorischen System, verschiedene Aspekte der prä- und postsynaptischen Entwicklung im MNTB zu verzögern oder aufzuhalten scheint, während Taubheit im Allgemeinen nur einen kleinen Effekt auf dessen Entwicklung zeigt.

I. INTRODUCTION

1. THE MAMMALIAN AUDITORY PATHWAY

Spatial hearing provides important cues for identifying dangers or prey and contributes to many social behaviors. Hence, the ability to localize a sound source rapidly and accurately is essential to the survival of many species. In contrast to the visual or somatosensory systems, there is no topographic representation of auditory space at the level of the sensory receptors in the inner ear. Instead, the mammalian central auditory system has evolved strategies to compute the location of a sound source by analyzing spectral cues and interaural differences (Grothe et al., 2010). To perform these tasks, auditory brainstem circuits feature several adaptations such as the ability to fire up to several hundred Hertz with high temporal precision and coincidence detection in the sub-millisecond range.

The peripheral auditory system

Sound waves cause vibrations of the tympanic membrane that are transmitted mechanically through the three middle ear ossicles (*malleus*, *incus* and *stapes*) and the oval window to evoke waves in the three fluid-filled chambers of the cochlea.

The *scala vestibuli* and *scala tympani* are filled with perilymph, a fluid with low potassium and high sodium concentration. In contrast, the endolymph of the *scala media* is rich in potassium, resulting in an ionic gradient that creates the endocochlear potential. An important component for the separation of these fluids are tight junctions, as they create a permeability barrier that regulates the flux of ions and larger solutes between the compartments (Madara, 1998).

Scala tympani and *scala media* are separated by the basilar membrane. The width and stiffness of this membrane decrease from the basal to the apical end of the cochlea, creating a gradient where the maximum amplitudes of the travelling wave occur at different locations along the membrane depending on the frequency (von Békésy, 1956). This topographic representation of frequencies, the so-called tonotopy, is maintained at nearly all stages of the auditory pathway.

Sitting on the basilar membrane is the organ of Corti, where the mechanical energy is transduced into electrical signals. Key components of the organ of Corti are two classes of mechanosensory cells, one row of inner hair cells (IHCs) and three rows of outer hair cells (OHCs). Auditory information about the environment is provided by IHCs while OHCs are involved in the amplification of sounds.

Both are equipped with a set of stereocilia at their apical end that extends above the reticular lamina into the endolymph. The tips of OHC stereocilia are attached to the tectorial membrane and accordingly, movements of the membrane relative to the hair bundle lead to a deflection of the stereocilia. The deflection of IHC cilia is caused by motion of the endolymph beneath the tectorial membrane. Stereocilia are connected with tip links that mechanically open or close cation channels when stretched, allowing ions to flow across the membrane, depolarizing the cell and thereby triggering the release of neurotransmitter at ribbon synapses with spiral ganglion neurons (Bear et al., 2007).

The central auditory system

Afferents from the spiral ganglion enter the brain via the 8th cranial nerve (vestibulocochlear nerve) and innervate the ventral and dorsal cochlear nucleus (VCN and DCN) in an organized projection pattern, preserving the tonotopic organization established in the cochlea. The VCN can be further divided into an anterior and posterior part (AVCN and PVCN, respectively) and is comprised of multiple specialized types of neurons that give rise to projections to nuclei throughout the brainstem (Cant and Benson, 2003). Thus, different aspects of auditory information can be extracted simultaneously in parallel ascending pathways (Bear et al., 2007).

One of the cell types found in the VCN are the octopus cells. Besides other targets, projections from the octopus area innervate the ventral nucleus of the lateral lemniscus (VNLL). VNLL neurons are contacted by several converging endbulb terminals (Covey and Casseday, 1986; Friauf and Ostwald, 1988; Adams, 1997; Schofield and Cant, 1997) and are capable of coincidence detection (Berger et al., 2014; Franzen et al., 2015). These neurons are broadly tuned and preferentially respond to the onset of sounds (Rhode et al., 1983; Covey and Casseday, 1991; Smith et al., 2005; Zhang and Kelly, 2006), and provide temporally precise feed-forward onset inhibition to the inferior colliculus (IC; Pollak et al. (2011)).

Other cell types of the VCN include the spherical and globular bushy cells (SBCs and GBCs, respectively), that convey information to several nuclei of the superior olivary complex (SOC), including the medial nucleus of the trapezoid body (MNTB) and the medial and lateral superior olive (MSO and LSO, respectively; Figure 1), that are involved in sound localization based on binaural cues (Cant and Benson, 2003).

Axons of superior olivary neurons then ascend via the lateral lemniscus and innervate the IC and other nuclei. The IC projects to the medial geniculate body in the thalamus that innervates the auditory cortex.

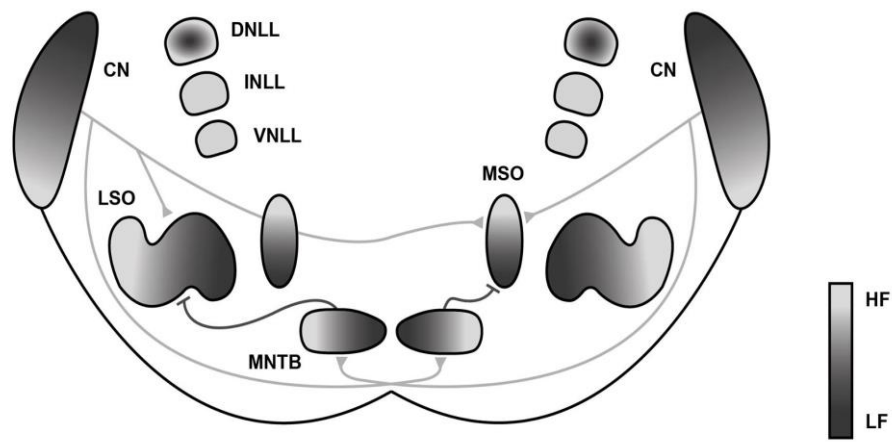


Figure 1: Schematic drawing of the mammalian auditory brainstem. Shown are the major nuclei of the auditory brainstem and the pathways involved in ILD and ITD processing. The gray gradient indicates the tonotopic organization of each nucleus (HF: high frequency, LF: low frequency). Excitatory projections are marked in grey, inhibitory projections in black. For clarity, only one side of each projection is shown. Medial superior olive (**MSO**) neurons receive bilateral excitatory input from the cochlear nucleus (**CN**) and inhibitory input from the ipsilateral medial nucleus of the trapezoid body (**MNTB**). Excitatory input to the lateral superior olive (**LSO**) is provided by the ipsilateral CN, inhibition arises from the ipsilateral MNTB. The MNTB receives excitatory input from the contralateral CN.

ITD and ILD coding in mammals

Unlike in the visual or somatosensory system, the cochlea provides no topographic map of auditory space. In order to obtain information about the location of a sound source nonetheless, the mammalian central auditory system analyzes spectral cues to localize sounds in the vertical dimension and compares differences in sound intensity and timing between the two ears for the localization in the horizontal plane (Grothe et al., 2010). Interaural level differences (ILDs) occur when the wavelengths is equal or shorter than the diameter of the head, hence ILDs are used to analyze high frequency sounds. For lower frequencies, the auditory system compares differences in the arrival times of a sound at the two ears (interaural time differences, ITDs).

The computation of ITDs and ILDs is performed in specialized nuclei of the superior olivary complex, the medial and lateral superior olive (MSO and LSO, respectively). Especially the MSO can show species-specific structural variations that reflect differences in hearing range when it is concerned with sound source localization. Low-frequency hearing animals such as the gerbil tend to have a large MSO, and it is less pronounced or strongly reduced in high-frequency hearing mammals like mice (Grothe, 2000; Tollin, 2003).

Both the LSO and the MSO receive inhibitory projections from the MNTB (Figure 1) that acts as a fast sign-inverting relay, providing well-timed glycinergic inhibition to these nuclei. The main input to the MNTB originates from GBCs in the AVCN that form specialized large axosomatic excitatory synapses with MNTB principal neurons, the calyces of Held. This largest central auditory synapse allows for fast and temporally precise high-frequency transmission (Borst and Sakmann, 1998).

The MSO is the major nucleus for ITD coding is able to perform coincidence detection of binaural inputs in the sub-millisecond range (Grothe et al., 2010). MSO neurons receive bilateral excitatory input from SBCs of both cochlea nuclei (Smith et al., 1993) as well as binaural inhibitory projections from the medial and lateral nucleus of the trapezoid body (Figure 1).

ILDs are processed in the LSO pathway. SBCs from the ipsilateral AVCN form excitatory synapses with LSO neurons. These neurons also receive inhibitory input from MNTB principal neurons that are innervated by GBCs from the contralateral AVCN (Figure 1). Depending on whether the sound intensity is higher at the contralateral or ipsilateral ear, the inhibitory or excitatory input predominates. Thus, the convergence of ipsilateral excitatory inputs and inhibition from the contralateral side provide the basis for ILD sensitivity (Boudreau and Tsuchitani, 1968, 1970; Moore and Caspary, 1983; Sanes, 1990; Kavanagh and Kelly, 1992; Grothe et al., 2010).

2. EARLY DEVELOPMENT AND REFINEMENT OF AUDITORY BRAINSTEM CIRCUITS

Auditory processing is a challenge that is reflected in the complex organization of the peripheral auditory system and the precisely arranged projections between multiple specialized nuclei throughout the brain. The basic circuitry in the auditory brainstem is established during fetal life and later refined by spontaneous and sensory-evoked activity (Friauf and Lohmann, 1999). The development of precisely organized projections is accompanied by changes at the synaptic level and a maturation of the intrinsic cell properties. Depending on the hearing range and the required temporal precision, the auditory system possesses species-specific differences regarding the developmental time course and further adaptations and refinements.

Early development of the auditory brainstem

The early mammalian brain consists of three primary vesicles, the prosencephalon, the mesencephalon and the rhombencephalon, which is divided into twelve domains, the rhombomeres (r) 1 – r11 and the isthmus (r0), that give rise to the different auditory brainstem nuclei. The subdivisions of the ventral CN originate from rhombomeres r2 to r4 and develop between embryonic day (E) 11 and E14 in mice. Most nuclei of the superior olivary complex are generated between E9 to E14 and descend from r5, with r3 additionally contributing to the MNTB. The nuclei of

the lateral lemniscus (NLL) arise from r4 (ventral NLL), r1 (intermediate NLL) and r0 (dorsal NLL). The IC is of mesencephalic origin (Di Bonito et al., 2013; Willaredt et al., 2015).

The growing axons in the developing auditory brainstem innervate their correct target nuclei with remarkable precision at early developmental stages and thus independent of spontaneous synaptic activity and sensory experience.

In mice, the subdivisions of the immature CN are innervated by auditory nerve fibers in a tonotopically organized pattern as early as E 15.5 (Kandler et al., 2009). It has been shown for rats that axons from CN neurons begin to innervate the nuclei of the superior olivary complex and the IC at E 18, and functional synapses are formed shortly after (Friauf and Lohmann, 1999). Tonotopy is established long before hearing onset and even before the onset of synaptic activity, indicating the importance of intrinsic programs (Koundakjian et al., 2007) and axonal guidance cues, such as Eph and Robo receptors and their ligands (Michalski et al., 2013; Cramer and Gabriele, 2014), for tonotopic map formation.

However, the maturation of auditory processing requires an additional reorganization and refinement of auditory brainstem circuits, as well as adjustments at the synaptic and cellular level.

Synaptic refinement in auditory brainstem nuclei

Neurons in the LSO encode ILDs by integrating converging excitatory projections from the ipsilateral CN with inhibitory glycinergic inputs provided by the MNTB. ILD coding requires the precise alignment of the two converging inputs so that LSO

neurons are excited and inhibited by the same sound frequency. This tonotopic organization is already present at hearing onset, however, projections are less precisely matched and the inhibitory input is more effective compared to adult animals (Sanes and Rubel, 1988).

The maturation of the inhibitory MNTB-LSO projection involves distinct periods of synapse silencing and axonal pruning. Pruning occurs after hearing onset and may contribute to the maturation of frequency selectivity by decreasing the spread of the dendritic arbor along the tonotopic axis (Sanes and Siverls, 1991; Sanes et al., 1992; Kandler et al., 2009).

Silencing occurs independent of auditory experience and is completed before hearing onset. During this period, LSO neurons become disconnected from the majority of their MNTB inputs, thus increasing the tonotopic precision of the MNTB-LSO projection (Kandler et al., 2009).

The developing central auditory system also exhibits fundamental differences in synaptic transmission compared to adult animals. As a result of the high intracellular chloride concentration in immature LSO neurons, the inhibitory neurotransmitters GABA and glycine act depolarizing and can elicit action potentials and activate voltage-gated calcium channels (Kandler and Friauf, 1995; Kotak et al., 1998; Kakazu et al., 1999; Kullmann and Kandler, 2001; Kullmann et al., 2002).

During development, the MNTB-LSO projection undergoes a gradual shift from primarily GABAergic to glycinergic transmission (Kotak et al., 1998; Nabekura et al., 2004) that is largely complete around hearing onset. The transient GABAergic phenotype may be important for the refinement of the projection since GABA can induce long-term depression at MNTB terminals (Kotak and Sanes, 2000; Chang et al., 2003).

MSO neurons analyze ITDs by comparing tonotopically matched bilateral excitatory inputs from both cochlear nuclei using a coincidence detection mechanism. They also receive bilateral inhibitory input from the MNTB and LNTB that contribute to ITD coding (Grothe, 2003; McAlpine and Grothe, 2003; Grothe et al., 2010). In mature low-frequency hearing animals, these inhibitory inputs are largely restricted to the soma, an organization that facilitates fast and temporally precise inhibition. The dendritic inhibitory inputs are selectively eliminated during development, a process that is dependent on auditory experience as it starts only after hearing onset and is impaired if normal acoustic input is not available (Kandler et al., 2009). In addition to the elimination of dendritic inputs, axonal pruning of MNTB projections to the MSO increases the tonotopic precision in this pathway (Werthat et al., 2008).

In contrast to the inhibitory pathway, the excitatory projections to the MSO are thought to show little or no refinement. In the intact auditory pathway, axon terminals from both cochlear nuclei contact dendrites of MSO neurons on opposing sides as soon as they innervate the MSO (Kil et al., 1995; Kitzes et al., 1995; Kapfer et al., 2002).

The MNTB is the major source of inhibitory input to the MSO and LSO. MNTB principal neurons receive glutamatergic input from GBCs in the contralateral CN. Each neuron is contacted by one single large axosomatic terminal, the calyx of Held, which functions as a fast, sign-inverting relay (Borst and Soria van Hoeve, 2012). The one-to-one innervation pattern is already largely present when the first protocalyces are discernable around P2 (Hoffpauir et al., 2006) and develops independent of spontaneous activity and auditory experience (Yousoufian et al., 2005). However, spontaneous activity is required for the establishment of a tonotopic gradient of intrinsic properties in MNTB principal neurons (Leao et al., 2006b) and influences the time course of maturation of the calyx of Held (Ford et al., 2009).

The transformation from an initially spoon-shaped calyx into a highly fenestrated structure occurs during the first three weeks of life and develops with a temporal gradient, beginning in the high frequency region of the MNTB. Animals deprived of auditory nerve activity do not exhibit such a gradient (Ford et al., 2009). The mature calyx shows membrane swellings that contain vesicles assembled around a cluster of mitochondria in a donut-like ring, in contrast to the more homogenous distribution of vesicles in pre-hearing animals (Wimmer et al., 2006).

The morphological changes in the calyx of Held are accompanied by functional changes underlying short term plasticity and the modulation of transmitter release, like a shortening of the presynaptic action potential waveform (Taschenberger and von Gersdorff, 2000) or differences in Ca^{2+} currents (Yang and Wang, 2006), Ca^{2+} channel subtype (Iwasaki and Takahashi, 1998) and Ca^{2+} domains (Wang et al., 2008).

Development of intrinsic cell properties

In addition to changes at the synaptic and connectivity level, the development of the auditory system involves the maturation of intrinsic passive and active properties of auditory brainstem neurons, such as the capacitance, the input resistance and the potassium currents.

Morphologically, a developmental reduction in soma size and dendritic arborization can be observed in neurons of many auditory brainstem nuclei (Rietzel and Friauf,

1998; Rautenberg et al., 2009; Franzen et al., 2015), leading to a decrease in effective cell capacitance and therefore, to a faster charging of the membrane. A developmental decrease in input resistance that was described for auditory neurons of several brainstem nuclei (Magnusson et al., 2005; Scott et al., 2005; Hoffpauir et al., 2010; Rusu and Borst, 2011; Walcher et al., 2011; Ammer et al., 2012; Franzen et al., 2015) can further shorten the integration time.

Beside these passive membrane parameters, a major component controlling the response properties of a neuron are voltage-gated potassium currents. These are also subject to developmental regulation and contribute to the maturation of action potential properties and the establishment of the adult firing behavior (Scott et al., 2005; Bortone et al., 2006; Franzen et al., 2015).

The interplay of the different intrinsic active and passive properties, together with refinements on the synaptic and circuit level, generate the basis for fast and precise voltage signaling that is required in binaural sound localization circuits.

3. MOUSE MODELS FOR HEARING DISORDERS

Hearing loss is the most common sensory loss in the human population, affecting approximately 1-2 out of 1000 newborns (Raviv et al., 2010). By the age of 70 years, the prevalence of a significant hearing loss of at least 25 dB increases to 60 % (Gratton and Vazquez, 2003).

The causes for hearing loss are manifold. A variety of environmental factors like noise exposure, acoustic trauma, infections or ototoxic drugs (Yorgason et al., 2006) can harm the auditory system. The prevalence of these acquired forms of hearing loss could be reduced by appropriate protection and avoidance of the risk factors. However, in up to 70 % of the cases, the hearing impairment is not induced by environmental influences but has a genetic basis (Raviv et al., 2010). To date, approximately 100 genes have been identified that are thought to be involved in the pathogenesis of different forms of hereditary hearing loss (Nishio et al., 2015). These show a large degree of clinical heterogeneity and can be classified into isolated non-syndromic forms and syndromic forms that are associated with other abnormalities (Raviv et al., 2010).

The mouse as a model for hearing loss

The heterogeneity of hereditary deafness reflects the complex interplay of the many genes that are involved in the development and function of the auditory system. Given the similarities between mice and humans regarding the cochlear transduction mechanism, mouse mutants represent a powerful model to identify and manipulate relevant genes and link them to their corresponding functions in hearing.

Today, a growing number of mouse models is available to study different developmental and functional aspects of auditory processing. Furthermore, these models allow for a detailed understanding of the underlying mechanisms of genetic hearing disorders in humans.

Broadly speaking, all mouse models fall in one of three categories – spontaneous mutations, mutations that are the result of exposure to mutagens, and approaches that target a certain gene directly (Brown et al., 2008).

Many spontaneous mutations were initially identified because they are often accompanied by vestibular dysfunctions that lead to characteristic behavioral abnormalities. Examples include the *shaker*, *whirler* and *waltzer* mutants that helped to reveal the roles of different proteins for the stereocilia bundle in the vestibular and auditory system (Gibson et al., 1995; Palma et al., 2001; Mburu et al., 2003).

An efficient method to create large numbers of novel mutations is the treatment with the highly potent mutagen N-ethyl-N-nitrosourea (ENU). ENU is known to generate point mutations that occur preferably at A-T base pairs (Brown and Peters,

1996). It acts most effectively in spermatogonial cells of male mice. The offspring of these mutagenized animals is then systematically screened for novel phenotypes. The advantage of this phenotype-driven approach is that it makes no *a priori* assumptions about the genes that may be involved and thus, it could uncover unexpected results (Nolan et al., 2000). Actually, this method revealed a phenotype that represents the first identified mutation of a microRNA associated with deafness, the *Diminuendo* mutant mouse (Lewis et al., 2009).

In a third gene-driven approach, mouse models are generated by directly manipulating or deleting a gene of interest in a permanent or conditional manner. An example is the Claudin-14-knockout mouse. The role of Claudin-14 for the hearing process was identified by the observation that mutations are associated with non-syndromic recessive deafness in humans (Wilcox et al., 2001; Lee et al., 2012; Charif et al., 2013). Furthermore, *in situ* hybridization and immunohistochemistry confirmed the expression of Claudin-14 in the organ of Corti. Targeted deletion of the gene resulted in a mouse model with a phenotype similar to the human phenotype (Ben-Yosef et al., 2003).

Genes and pathways involved in hearing disorders

Mouse models exist for numerous aspects of the hearing process and have helped to increase our understanding of the underlying mechanisms and the involved genes and molecules.

Mapping of deafness genes in human families as well as the analysis of mouse mutants associated with a deaf phenotype have revealed various molecular

pathways that affect different components of the peripheral and central auditory system, including fluid homeostasis and compartmentalization, gene regulation and synaptic transmission (Dror and Avraham, 2010).

The fluids that fill the compartments of the inner ear are an essential for normal hearing as they transfer the sound pressure wave, leading to a deflection of the stereocilia. The high potassium concentration of the endolymph creates an ion gradient that enables a depolarization of the hair cell upon mechanical stimulation. A large number of proteins are involved in establishing and maintaining the ionic compositions of the fluids, including channels, transporters and tight junction (TJ) proteins that form a diffusion barrier between the compartments of the inner ear. Mutations in these genes are associated with a variety of syndromic and non-syndromic hearing disorders (Dror and Avraham, 2010).

The most common forms of autosomal recessive deafness in humans, DFNB1A and DFNB1B, result from mutations in genes encoding for connexins (Kelsell et al., 1997; del Castillo et al., 2002). Connexins are components of gap junctions that are thought to play a crucial role for potassium redistribution in the inner ear (Nickel and Forge, 2008).

Transducing the mechanical wave into an electrical signal requires functional hair cells and the structural integrity of the basilar and tectorial membranes. Numerous proteins have been identified that are essential for the structure and function of the signal transduction machinery, including scaffold proteins, motor proteins and adhesion molecules (Dror and Avraham, 2010). Many of them are associated with different forms of deafness like the clinically and genetically heterogeneous Usher syndrome, the most common form of deaf-blindness. At least twelve genes code for components of a larger multiprotein complex, that participates in the

development and function of sensory cells in the inner ear and the retina (Kremer et al., 2006; Mathur and Yang, 2015)

While most forms of genetic hearing disorders are a consequence of impaired hair cell function, there are also less frequent conditions in which the transmission from the cochlea to the brain is disrupted (Dror and Avraham, 2010). Examples for proteins known to be involved in signal transmission at the ribbon synapses of IHCs are VGLUT3 and otoferlin. Mutations in the gene encoding for the vesicular glutamate transporter VGLUT3, responsible for the accumulation of glutamate in synaptic vesicles, are the cause of the human hearing disorder DFNA25 (Ruel et al., 2008). Otoferlin has been shown to be essential for vesicle exocytosis, as it serves as the major Ca^{2+} sensor at ribbon synapses and interacts with proteins of the SNARE complex (Roux et al., 2006). Mutations are linked to the human auditory neuropathy DFNB9 (Yasunaga et al., 1999).

The correct temporal and spatial expression pattern of genes is essential for development and function of the nervous system. The transcription of genes into RNA molecules is controlled by regulatory proteins like transcription factors (TF), and a further posttranscriptional regulation of gene expression is accomplished by microRNAs. Mutations in TF genes are associated with various developmental defects of the inner ear (Dror and Avraham, 2010) and the central auditory system (Willaredt et al., 2015), causing different syndromic and non-syndromic forms of hereditary hearing loss in humans and mice.

The role of miRNAs for the development and function of the auditory system was first described by two complementary studies that link mutations in the seed region of microRNA-96 (miR-96) to a hearing impaired phenotype in humans (Mencia et al., 2009) and in the so-called *Diminuendo* mouse (Lewis et al., 2009).

The Diminuendo mouse

The *Diminuendo* phenotype results from a point mutation in the seed region of miR-96. MicroRNAs are small non-coding RNAs with a length of about 21-23 nucleotides involved in the regulation of gene expression by influencing mRNA stability and translation. Since their discovery in *Caenorhabditis elegans*, hundreds of microRNAs have been identified in a large variety of metazoa (Grimson et al., 2008). They are thought to regulate the expression of most mammalian genes (Friedman et al., 2009) and are involved in many cellular programs, including proliferation, differentiation and apoptosis in various tissues. Alterations are associated with developmental defects, cancer and other diseases (Ruepp et al., 2010; Tuna et al., 2016). They also play a key role in the brain, as they coordinate the precise spatial and temporal expression of numerous genes that generate the anatomical and functional complexity of the central nervous system. (Davis et al., 2015).

Their biogenesis begins with the transcription of primary miRNA by Polymerase II from the corresponding gene. It is further processed by the enzymes Drosha and Dicer, resulting in a single-stranded miRNA molecule that is incorporated in the RNA-induced silencing complex (RISC). The single strand acts as a template for the RISC to recognize the complementary sequence of the target mRNA. Mutations in miRNAs lead to impaired target recognition and thus, their regulatory role in gene expression is impaired (Kloosterman and Plasterk, 2006; Winter et al., 2009).

MiR-96 is expressed in all sensory hair cells of the inner ear and in cochlear and vestibular ganglion neurons of newborn mice, affecting the expression of various genes directly or as a downstream effect at specific developmental stages. Some of the downregulated genes are highly expressed in hair cells and are partly known to cause deafness in the corresponding knockout, including the motor protein Prestin,

the calcium-binding protein Oncomodulin, both expressed in OHCs, and Ptpdq that is required for hair cell maturation (Lewis et al., 2009).

The *Diminuendo* phenotype is characterized by progressive hearing loss in heterozygous and profound congenital deafness in homozygous animals. Deafness is a consequence of an arrested development of cochlear hair cells around birth and their subsequent degeneration around postnatal day (P) 7. Hair cells fail to differentiate into IHCs and OHCs and show no maturation of their biophysical and morphological properties (Kuhn et al., 2011).

A recent study also demonstrated a developmentally increasing expression of miR-96 in the brainstem (Rosengauer et al., 2012), suggesting a possible role of miR-96 for the development and maturation of the central auditory brainstem as well. As there is no conditional knockout for miRNA-96 in the brainstem available yet, the Claudin-14-knockout mouse serves as a control in this study.

The Claudin-14-knockout mouse

Mutations in the gene encoding for Claudin-14 have been linked to an autosomal-recessive form of non-syndromic hearing loss in humans, DFNB29 (Wilcox et al., 2001; Lee et al., 2012; Charif et al., 2013).

The creation of a Claudin-14 knockout mouse demonstrated that deafness is a result of hair cell degeneration during the first three weeks of life in homozygous mutants (Ben-Yosef et al., 2003). Claudin-14 is a tight junction protein that is expressed in the cochlea (Wilcox et al., 2001; Ben-Yosef et al., 2003).

Tight junctions are important to create a permeability barrier that regulates the flux of ions and larger solutes between compartments with different ionic compositions (Madara, 1998). In the inner ear, tight junctions separate the compartments containing the sodium-rich perilymph and the potassium-rich endolymph (Bear et al., 2007). In vitro experiments have demonstrated that the absence of Claudin-14 from tight junctions results in a failure to maintain the paracellular cation-selective barrier of the reticular lamina. The beginning of OHC loss around P 9 coincides with the increase of endolymphatic potassium concentration and the establishment of the endocochlear potential. Presumably, the exposure of the basolateral membrane of OHCs to toxic potassium concentrations is responsible for their degeneration, since the elevated potassium concentration leads to prolonged depolarizations of OHCs which eventually causes their death. (Ben-Yosef et al., 2003).

The rapid loss of OHCs is followed by a slower degeneration of IHCs. Measurements of auditory brainstem responses at P 15 – P 17 demonstrate that *Cldn-14^{-/-}* mice are deaf (Ben-Yosef et al., 2003).

A possible explanation for the lower sensitivity of IHCs to the knockout is that they are able to substitute Claudin-14 with other members of the Claudin family, similar

to other Claudin-14 expressing tissues. In the liver, the kidney and the vestibular system, the knockout does not affect the function because other Claudins can compensate for the loss (Hou, 2012).

In addition, the basolateral membrane of IHCs is not exposed to a fluid-filled space. IHCs are therefore possibly less sensitive to alterations of the ionic composition and thus, degenerate later (Ben-Yosef et al., 2003).

4. AIMS

1. ILD coding requires the converging excitatory and inhibitory inputs to the LSO to be tonotopically organized and matched precisely. The adjustment of the inhibitory MNTB-LSO projection is largely accomplished before hearing onset. In rats, this projection is thought to undergo a shift from predominantly GABAergic to glycinergic transmission.

In this project, this developmental switch in transmitter was studied in pre-hearing mice and gerbils. The comparison of high- and low-frequency hearing animals also may allow to identify adaptations of inhibitory sound localization circuits depending on the different requirements of the system.

2. Principal neurons in the LSO process ILDs by integrating ipsilateral excitatory inputs with inhibitory inputs coming from the contralateral side. These converging inputs are tonotopically organized: LSO neurons in the medial limb are more sensitive to high frequency sounds while cells located laterally rather respond to low frequencies (Tollin, 2003).

This project addresses the question whether the tonotopic gradient in the adult mouse LSO is reflected in adaptations in the intrinsic and synaptic properties of neurons depending on their position within this nucleus.

3. Normal development of the central auditory system requires a combination of genetically encoded programs and activity-dependent mechanisms. Mouse models provide a powerful tool to analyze the genetic and molecular basis of hearing and help to understand the fundamental mechanisms of auditory development and function.

The majority of mutations that are known to cause early-onset deafness usually lead to various structural and functional defects of the cochlea (Richardson et al., 2011). The *Diminuendo* mutation, a single base change in miR-96 is an exception. Besides leading to an arrest of cochlear hair cell development, it is also expressed in the brainstem (Rosengauer et al., 2012), but its role for the maturation of the central auditory system is not known.

The aim of this project was to study the consequences of the *Diminuendo* mutation for auditory processing by analyzing morphological and functional changes occurring at MNTB principal neurons and their calyx of Held-synapses in adult mice.

To be able to distinguish between effects that originate in the central nervous system and the consequences of deafness in general, the *Diminuendo* mouse was compared to another mutation that serves as a model for peripheral hearing loss only, the Claudin-14-knockout mouse. The knockout of this tight junction protein results in a degeneration of OHCs and IHCs during the first three weeks of life (Ben-Yosef et al., 2003). Thus, the Claudin-14-knockout mouse is a suitable control since both mouse models display a normal initial development of the cochlea that is followed by a degeneration of hair cells.

II. MATERIAL AND METHODS

1. ANIMALS

All experiments complied with institutional guidelines and national and regional laws as approved by the Regierung of Oberbayern. Experiments were performed on male and female Mongolian Gerbils (*Meriones unguiculatus*) and mice aged between P5 and P30. Mouse lines used were C57BL/6N (Chapter III-1 and III-0), Claudin-14 knockout (Cldn-14^{-/-}) mice on a NMRI background, and *Diminuendo* (dmdo/dmdo) mice on a C3HeB/FeJ background (Chapter III-3). For Cldn-14^{-/-} and dmdo/dmdo mice, their respective wild type littermates served as controls. The Claudin-14 and *Diminuendo* animals were supplied by the group of Prof. Dr. Nothwang (Carl von Ossietzky Universität Oldenburg, Institut für Biologie und Umweltwissenschaften), who also were responsible for the genotyping.

2. SLICE PREPARATION

Similar to Berger et al. (2014) and Franzen et al. (2015), brains were removed after decapitation under isoflurane anesthesia and transferred to ice cold slice solution containing (in mM) 50 sucrose, 25 NaCl, 27 NaHCO₃, 2.5 KCL, 1.25 Na₂HPO₄, 3 MgCl₂,

0.1 CaCl₂, 25 glucose, 0.4 ascorbic acid, 3 myo-inositol and 2 Na-pyruvate, bubbled with 95% O₂ and 5% CO₂, pH 7.4. 200 µm-thick transverse brain slices containing the LSO or the MNTB were taken with a VT1200S vibratome (Leica Biosystems, Germany) and incubated in recording solution (same as slice solution but with 1.2 mM CaCl (Chapter III-2 and III-3) or 2 mM CaCl (Chapter III-1), 1mM MgCl₂, 125 mM NaCl and no sucrose) at 35°C for 45 minutes, bubbled with 5% CO₂ and 95% O₂.

3. ELECTROPHYSIOLOGY

All electrophysiological experiments were carried out near physiological temperature (34-36°C) and slices were continuously perfused with recording solution. Cells were visualized and imaged using a BX50WI Microscope (Olympus, Germany) equipped with gradient contrast illumination and a TILL photonics system consisting of a TILL-Imago CCD camera and a monochromator (Polychrome IV; TILL Photonics, Germany). Recordings were performed with an EPC10/2 amplifier (HEKA Elektronik, Germany) with a sampling frequency of 50 kHz (Chapter III-2 and III-3) or 100 kHz (Chapter III-1).

In voltage-clamp experiments, access resistance was compensated to 3 MΩ. For current-clamp recordings the bridge balance was set to 100 %. Patch pipettes of 3-3.5 MΩ resistance were pulled from borosilicate glass capillaries using a DMZ Universal Puller (Zeitz Instruments, Germany) and filled with an intracellular solution.

For voltage-clamp experiments the solution contained (in mM): 105 Cs-gluconate, 26.7 CsCl, 10 Cs-HEPES, 20 TEA-Cl, 3.3 MgCl₂, 2 Na₂-ATP, 0.3 Na-GTP, 3 Na₂-

phosphocreatine, 5 Cs-EGTA, 5 QX 314-bromide and 20 μM Alexa 568. The pH was adjusted to 7.2 with CsOH.

For current-clamp experiments the following intracellular solution was used (in mM): 145 K-gluconate, 5 KCl, 15 HEPES, 2 K-ATP, 2 Mg-ATP, 0.3 Na-GTP, 7.5 Na₂-phosphocreatine, 5 K-EGTA and 20 μM Alexa 568, adjusted to pH 7.2 with KOH.

Synaptic inputs were stimulated either with a glass electrode filled with recording solution or with a concentric bipolar electrode (FHC, USA). A 200- μs biphasic voltage pulse with adjustable stimulation strength was triggered by the amplifier and conveyed by an isolated pulse stimulator (Model 2100, A-M Systems, USA). To activate the inputs to the MNTB, the electrode was placed medial to the MNTB. Synaptic currents in the LSO were evoked by stimulating the fibers projecting from the MNTB to the LSO.

Excitatory and inhibitory inputs were pharmacologically isolated by adding 10 μM SR-95531 and 1 μM Strychnine or 20 μM DNQX and 10 μM R-CPP, respectively. Miniature postsynaptic currents were measured in the presence of 1 μM TTX. Data are not corrected for liquid junction potential.

4. IMMUNOHISTOCHEMISTRY AND CONFOCAL MICROSCOPY

After inducing a deep anesthesia with 200 mg/kg pentobarbital, animals were perfused transcardially with Ringer solution containing 0.1% Heparin for 5 minutes, followed by 4% paraformaldehyde (PFA) for 30 minutes. Brains were post-fixed overnight in 4 % PFA at 4°C and 50 - 70 μm -thick coronal sections were cut with a

VT 1200S vibratome (Leica Biosystems, Germany). After rinsing in phosphate-buffered saline (PBS, pH 7.4) sections were transferred to blocking solution containing 1 % bovine serum albumin, 0.3% Triton X-100 and 0.1% Saponin in PBS. Standard immunohistochemical procedures were performed on free-floating slices with primary antibodies for microtubule-associated protein 2 (MAP2, chicken polyclonal, 1:1000, Neuromics, USA) and synaptic vesicle protein 2 (SV2, mouse monoclonal, 1:500, DSHB, USA). After 2 days of incubation at 4°C, secondary antibodies (Alexa488 donkey anti-chicken, 1:200 and Cy3 donkey anti-mouse, 1:300, Dianova, Germany) were applied for 2 hours at room temperature.

Slices were mounted in Vectashield medium and confocal scans were acquired with a Leica TCS SP5-2 confocal laser scanning microscope (Leica Microsystems, Germany). Images were taken with a 63x objective (1.32 NA), leading to a pixel size between 120 nm² and 320 nm², depending on the zoom factor. To improve the signal-to-noise ratio, images were averaged from 6 to 8 successive scans (Chapter III-3).

5. IMAGE AND DATA ANALYSIS

Confocal image stacks were processed and analyzed with ImageJ. To estimate the cell diameter of MNTB neurons (Chapter III-3), the length and width of each cell was measured from maximum intensity projection images of the MAP2 stainings. To quantify structural changes at the calyx of Held, the donut-like substructures were extracted from maximum projections and the grey value of individual donuts was determined by line scans and normalized over the dynamic range.

Analysis of electrophysiological data was performed offline using custom-written IGOR Pro procedures (WaveMetrics, USA), Microsoft Office Excel (Microsoft, USA) and GraphPad InStat (GraphPad Software, USA). Results are presented as mean \pm SEM. Data were tested for normality using a Shapiro-Wilk test. Since the majority of data was considered to follow a normal distribution, statistical significance was determined by a paired or unpaired two-tailed Student's t-test with a significance level of $P < 0.05$. In no case, using the Mann-Whitney-U test would have changed the significance level. Correlation coefficients were determined by a Pearson test (Chapter III-2)

III. RESULTS

1. DEVELOPMENT OF GABAERGIC AND GLYCINERGIC INPUTS TO THE LSO IN MICE AND GERBILS.

A strategy for the localization of high-frequency sounds in the horizontal plane is the comparison of interaural level differences that are processed in the lateral superior olive. The LSO integrates excitatory inputs from the ipsilateral anteroventral cochlear nucleus with contralateral inhibitory inputs provided by the medial nucleus of the trapezoid body. ILD coding requires both inputs to be tonotopically organized and matched precisely.

The adjustment of the inhibitory MNTB-LSO projection is largely accomplished before hearing onset, thus largely independent of sound-evoked activity and genetically encoded (Kandler et al., 2009). During early postnatal development, this projection undergoes a shift from predominantly GABAergic to glycinergic transmission, a process that is thought to contribute to the refinement of the MNTB-LSO pathway (Kotak et al., 1998; Korada and Schwartz, 1999; Nabekura et al., 2004; Weber et al., 2015). For isolated neurons of developing rats, the co-release of GABA and Glycine from single vesicles has been demonstrated (Nabekura et al., 2004).

In the following, I studied the experience-independent, genetically encoded early postnatal development of the inhibitory MNTB-LSO projection in mice and gerbils, two species with different hearing ranges. The comparison of both rodents may help to identify adjustments of sound localization circuits to the varying demands of high- and low-frequency hearing animals.

To comparatively characterize the development of the inhibitory projection, evoked and miniature inhibitory postsynaptic currents (IPSCs) were analyzed. With the aim to separate between GABAergic and glycinergic transmission, all experiments were performed in the absence and presence of the GABA_A receptor antagonist SR-95531.

Considering the different hearing ranges of the two species and the tonotopic gradient in the LSO, I focused on the medial limb of the nucleus which displays greater sensitivity to high frequency sounds.

Miniature IPSCs before and after hearing onset

Pharmacologically isolated miniature IPSCs (mIPSCs) were measured from mice and gerbils at the ages of P8-9 and P15-16 and were analyzed concerning their amplitudes, decay times and frequencies. I included only cells that had a minimum of 50 mIPSCs and were recorded for at least 3 minutes without and in the presence of SR-95531. As an additional control, Strychnine was also added in some cases, resulting in the complete absence of mIPSCs, proving that all observed miniature events were GABA- and glycinergic.

The very low mIPSC frequency in animals aged P 6 or younger prevented further analysis of this age group.

Since most mIPSCs showed no clear bi-exponential decay time course, the decay times shown in Figure 2A were obtained from mono-exponential functions fitted to the average mIPSCs of the respective cells before and after the wash-in of SR-95531. In contrast to the idea of co-release (Nabekura et al., 2004), the GABA_A blocker did not have any effect on the decay kinetics of both species and age groups.

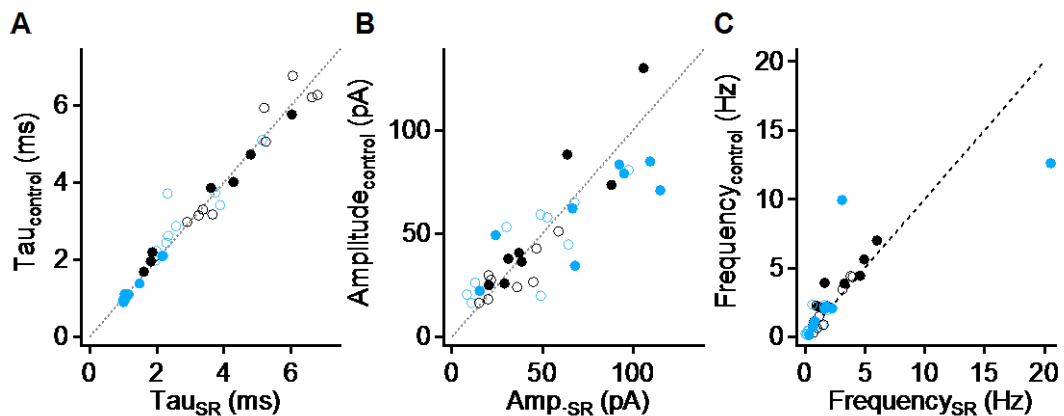


Figure 2: mIPSCs in the developing LSO of mice and gerbils. Decay time constants (A), amplitudes (B) and frequency (C) of miniature IPSCs under control conditions and in the presence of SR-95531. Blue open circles: gerbil P 8-9 (n = 10); black open circles: mouse P 8-9 (n = 10); blue closed circles: gerbil P 15-16 (n = 8); black closed circles: mouse P 15-16 (n = 8).

However, the analysis demonstrates interesting differences between mice and gerbils. In the gerbil, the average mIPSC had a decay time of 3.02 ± 0.31 ms at the age of P 8-9 that accelerated significantly ($p < 0.0005$) to 1.19 ± 0.14 ms at postnatal day 15-16. Miniature IPSCs in mice were with 4.49 ± 0.55 (P 8-9) and 3.15 ± 0.59 (P 15-16, $p = 0.06$) generally slower than in Gerbils.

Shown in Figure 2B are the median mIPSC amplitudes for each cell with and without blocked GABA_A currents. Again, the bath application of SR-95531 did not lead to significant changes. The comparison of the two animal species revealed larger mIPSCs in the gerbil and in both species, the amplitude increased during development (mouse: -29.51 ± 4.19 (P 8-9), -57.23 ± 13.14 pA (P 15-16), $p = 0.06$.; gerbil: -44.37 ± -7.09 (P 8-9) and -60.80 ± -8.28 pA (P 15-16), $p < 0.0005$). This increase in amplitude was accompanied by a slightly elevated mIPSC frequency (Figure 2C). In the young age group, an average of 0.99 ± 0.28 (gerbil) and 2.10 ± 0.48 (mouse) inhibitory events per second were recorded that increased to 3.85 ± 1.66 (gerbil, $p = 0.10$) and 3.90 ± 1.66 (mouse, $p = 0.24$) IPSCs per second at the age of P 15-16. In none of the groups the frequency was sensitive to the application of SR-95531.

To summarize, the study demonstrated species-specific differences with faster mIPSC kinetics and larger amplitudes in gerbils. During development, mIPSCs in both animals develop faster kinetics, larger amplitudes and a higher frequency. Unexpectedly, the bath application of the GABA_A receptor antagonist SR-95531 failed to modify the shape or frequency of the miniature inhibitory events although GABAergic and glycinergic co-release has been indicated to occur at the MNTB-LSO projection (Nabekura et al., 2004). Thus, these results speak against the release of both transmitters from the same vesicle in mice and gerbils. To address this issue

further, I next studied IPSCs evoked by stimulations of the inhibitory inputs to the LSO.

Evoked IPSCs in prehearing mice and gerbils

To evoke IPSCs, a bipolar stimulation electrode was placed in the fibers projecting from the MNTB to the LSO of mice and gerbils at the ages of P 5-6 and P 8-9. Excitatory currents were blocked pharmacologically.

Figure 3A shows the average IPSCs calculated from ten repetitions under control conditions and under the presence of SR-95531. In all groups, the average amplitudes showed a slight decrease after the wash-in of the GABA_A receptor blocker. This effect was more pronounced in gerbils and independent of the age (mice P 5-6: control: -0.51 ± 0.17 nA, SR: -0.47 ± 0.19 nA (-5.7 %; $p = 0.57$); mice P 8-9: control -1.71 ± 0.34 nA, SR: -1.61 ± 0.31 nA (-6.2 %; $p = 0.33$); gerbil P 5-6: control: -4.18 ± 2.34 nA, SR: -3.57 ± 1.79 nA (-14.7 %; $p = 0.46$); gerbil P 8-9: control: -4.47 ± 1.44 , SR: -3.83 ± 0.80 nA (-14.2 %; $p = 0.56$; Figure 3B).

Double exponential functions were fitted to each IPSC to extract the fast and slow components of the decay time constants. The fast component was not sensitive to SR-95531. In P 5-6 mice, τ_{fast} was on average 7.11 ± 0.86 ms under control conditions and 7.21 ± 0.83 ms in the presence of the drug ($p = 0.83$). At the age of P8-9, τ_{fast} decreased to 4.37 ± 0.69 ms (control) and 4.32 ± 0.61 ms (SR; $p = 0.83$). For the P 5-6 gerbils, values of 4.43 ± 0.69 ms (control) and 4.47 ± 0.72 ms were determined ($p = 0.30$). In the older age group τ_{fast} was reduced to 2.91 ± 0.29 and 3.07 ± 0.32 ms before and after the application of SR-95531 ($p = 0.21$; Figure 3C).

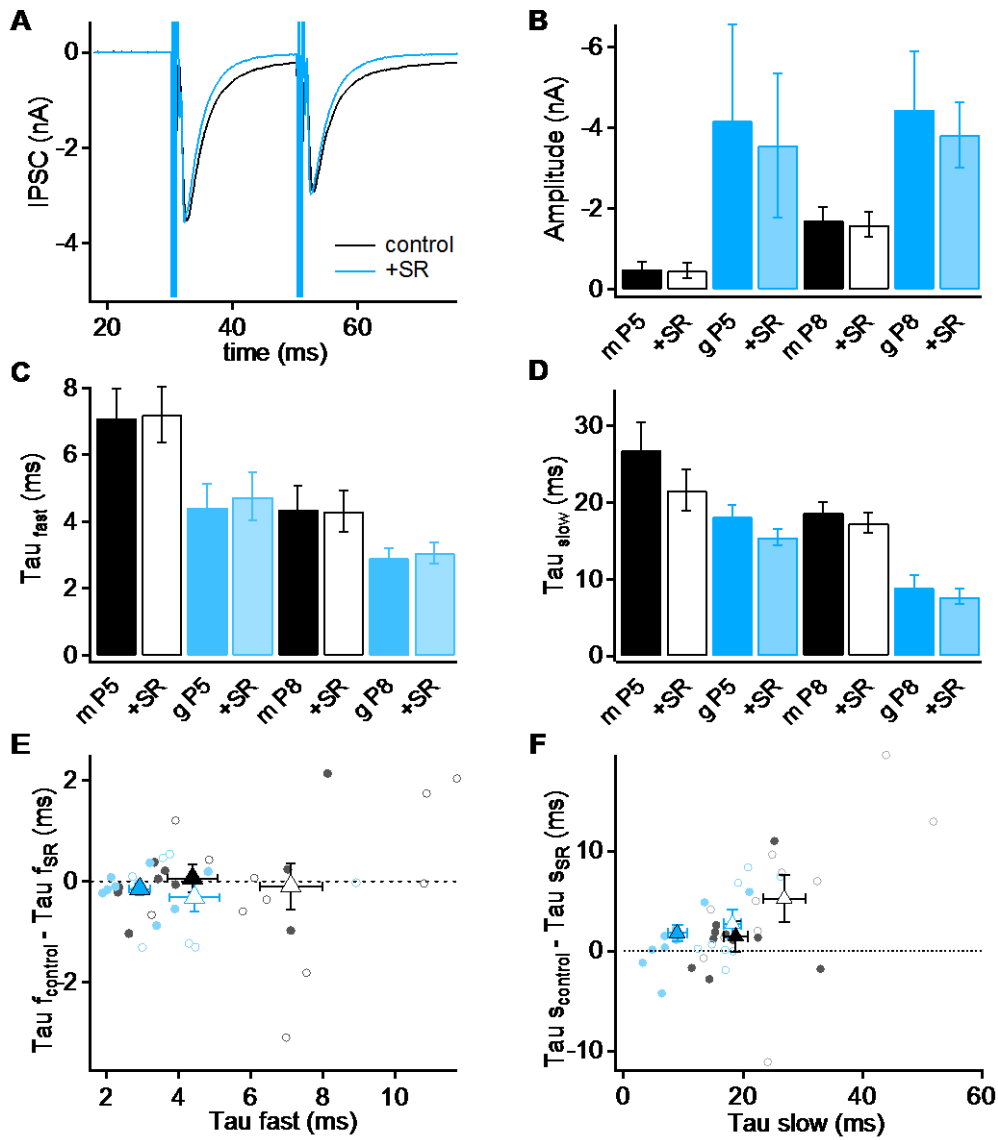


Figure 3: evoked IPSCs in pre-hearing mice and gerbils. **A:** example IPSC under control conditions (black) and after SR-95531 bath application. **B, C, D:** IPSC amplitudes (**B**), τ_{fast} (**C**) and τ_{slow} (**D**) in mice and gerbils at the ages of P 5-6 and P 8-9 before and after the wash-in of SR-95531. **E, F:** change in τ_{fast} (**E**) or τ_{slow} (**F**) plotted against the initial value. Blue open circles: gerbil P 5-6 (n = 9); black open circles: mouse P 5-6 (n = 11); blue closed circles: gerbil P 8-9 (n = 10), black closed circles: mouse P 8-9 (n = 10). Triangular symbols indicate average values.

While the fast component is unchanged by the block of GABA_A receptors, the drug appears to have an influence on the slow component shown in Figure 3D. The effect was strongest in the younger mice with a reduction of 19.6 % from 26.86 ± 3.59 ms to 21.61 ± 2.38 ms ($p = 0.05$). In P 8-9 mice, τ_{slow} slightly decreased from 18.76 ± 2.03 ms to 17.30 ± 2.10 ms (-7.8 %; $p = 0.26$). In gerbils, the slow component was insignificantly reduced from 18.2 ± 1.47 to 15.49 ± 1.08 ms (-14.9 %; $p = 0.10$) at the age of P 5-6. IPSCs in the older animals showed a similar decrease from 8.94 ± 1.60 to 7.74 ± 1.81 ms (-13.5 %; $p = 0.22$).

Figure 3E and F illustrate the effect of SR-95531 on the decay time constants by plotting the change in τ against its initial value. While τ_{fast} remained constant, the slow component displayed a sensitivity to the drug that seems to have a stronger effect on IPSCs with a larger τ_{slow} .

Unlike the analysis of mIPSCs, the fiber stimulation experiment might provide indication for the release of both GABA and glycine at LSO neurons. Evoked IPSCs showed a biphasic decay that suggests the involvement of inhibitory conductances with different kinetics that were modified by the GABA_A receptor antagonist SR-95531. The stronger influence on IPSCs in younger animals would be consistent with the developmental switch from GABAergic to glycinergic transmission in the LSO. However, these results provide no evidence for the co-release of GABA and Glycine from single vesicles in mice and gerbils, contrary to the rat (Nabekura et al., 2004). Therefore, the data suggest that the switch in transmitter type must be based on a different cellular mechanism other than co-release.

2. CHARACTERIZATION OF CELLS AND INPUTS IN THE ADULT MOUSE LSO ALONG THE TONOTOPIC AXIS

After hearing onset, the integration of ipsilateral excitatory inputs and contralateral inhibitory inputs enables LSO neurons to encode interaural differences in sound intensity. This subtraction mechanism requires the inputs to be matched regarding their frequency tuning, resulting in a tonotopic organization of the LSO with neurons preferentially responding to high frequencies in the medial limb and cells more sensitive to lower-frequency sounds located in the lateral part (Tollin, 2003).

The hearing range of mice is limited to relatively high frequencies above 2 kHz (Heffner and Heffner, 2007). The following experiments investigated whether the tonotopic gradient in the mature mouse LSO is accompanied by adaptations in the intrinsic and synaptic properties of neurons sensitive to different frequencies. To answer this question, I performed whole-cell recordings of neurons along the tonotopic axis in the LSO of adult mice (P 20-30). I characterized their passive and active properties that determine how the cell responds to the incoming inputs. Excitatory and inhibitory synaptic transmission was studied by analyzing miniature and evoked postsynaptic currents.

Characterization of passive and active properties of LSO neurons

Figure 4A shows an exemplary neuron (left) and its position in the LSO (right). The position for each cell was mapped on a stereotypic LSO (Figure 4B) to reveal possible differences in passive and active membrane properties along the tonotopic axis.

Passive membrane parameters such as the input resistance (R_{in}), the membrane time constant (τ) and the cell capacitance (C_m) contribute to signal transmission by influencing the integration of synaptic inputs and interacting with the active properties of the neuron. These parameters can be approximated by analyzing the voltage responses to current injections that are kept small to minimize the additional activation and deactivation of voltage-dependent conductances (Ammer et al., 2012; Berger et al., 2014; Franzen et al., 2015).

Fehler! Verweisquelle konnte nicht gefunden werden. Figure 4B shows the voltage deflection induced by the injection of 500 ms-long currents of -5 pA. τ , extracted from exponential functions fitted to the onset response, was used to estimate the membrane capacitance. R_{in} did not correlate with the membrane capacitance (correlation coefficient $r = 0.42$) but there appeared to be two different populations of neurons, one with rather low R_{in} and one with input resistances above 500 M Ω (Figure 4C). Neurons with a R_{in} above 500 M Ω were predominantly found in the medial and middle parts of the LSO (Figure 4E, top graph). The population with input resistances below 500 M Ω , enlarged in Figure 4E (second to top), exhibited an increasing R_{in} from the medial to the lateral side of the LSO, with an average R_{in} of 32.28 ± 3.42 M Ω for the ten most medial neurons and 86.63 ± 14.43 M Ω for the ten most lateral neurons ($p < 0.002$).

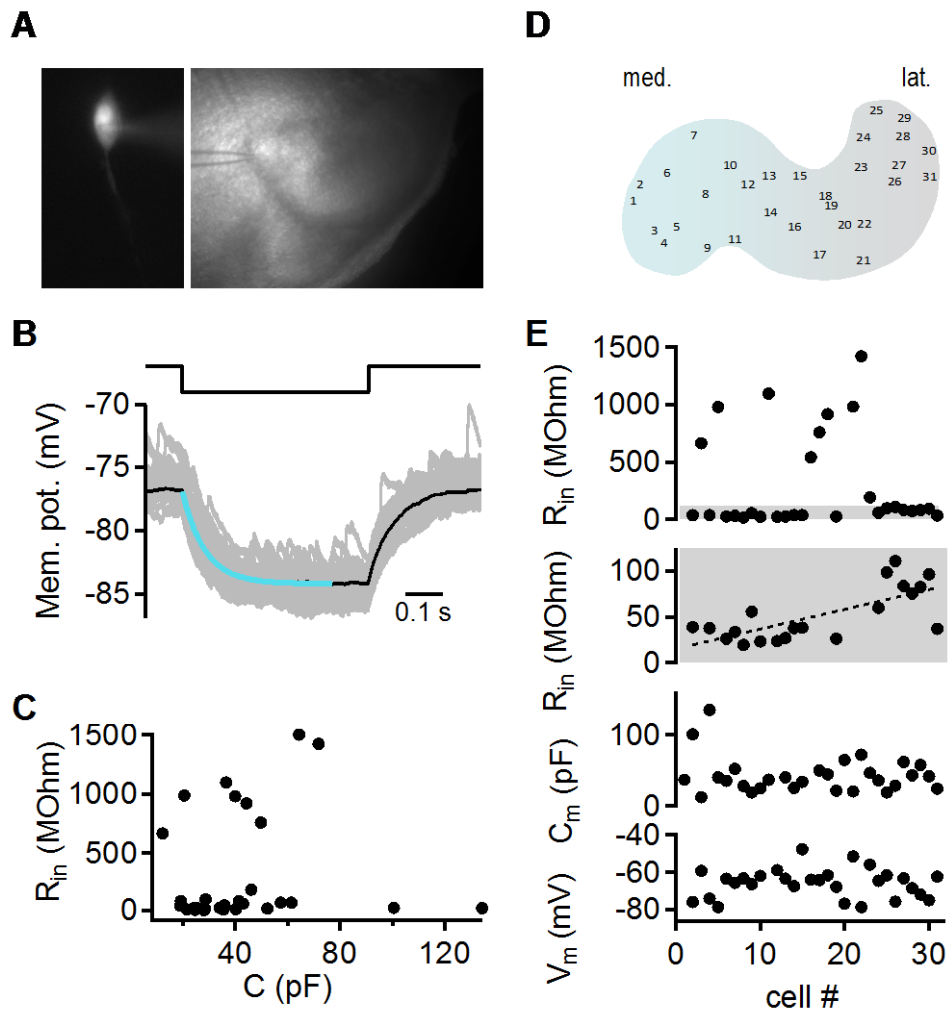


Figure 4: Passive properties of LSO neurons. **A:** example neuron filled with Alexa dye (left) and its location in the LSO (right). **B:** membrane potential changes in response to 500 ms-long current injections (top). 60 single trials (grey) were averaged (black) and fitted with an exponential function (blue). **C:** R_{in} as a function of the membrane capacitance. **D:** Schematic illustration of the LSO. Numbers indicate the location of each recorded cell. **E:** Membrane parameters R_{in} , C_m and V_m plotted according to the position of the respective cell in the LSO. For R_{in} (top panel), the area labeled in grey is shown enlarged, the dotted line indicates the linear regression of R_{in} dependent on the cell's position (second to top). Included are the pooled data of onset and sustained firing neurons. $n = 31$

The membrane capacitance and the resting membrane potential V_m displayed no position-dependent differences (Figure 4E, bottom panels). On average, the neurons had a C_m of 41.60 ± 4.41 pF and a resting membrane potential of -67.53 ± 15.05 mV.

Characterization of the firing behavior in response to 500 ms-long current injections between -200 and +1000 pA confirmed the existence of two different populations. About two-thirds of neurons fired 1-3 onset action potentials (Figure 5A, top) while the second type displayed a sustained firing pattern (Figure 5A, bottom).

With an average R_{in} of 815.04 ± 148.05 M Ω , the continuously firing neurons were equivalent to the high input resistance cells shown in Figure 4C and 4E and differed significantly from neurons firing an onset action potential ($R_{in} = 46.89 \pm 6.00$ M Ω ; $p < 0.0005$). In contrast to continuously spiking neurons, the steady state current in onset neurons changes linear with the injected current (Figure 5B).

However, under physiological conditions action potentials are rather elicited by short excitatory postsynaptic currents than by prolonged constant current injections. Thus, I used a stimulus approximating the shape of an EPSC with a rise time of 150 μ s and a decay time of 800 μ s that was incremented in steps of 100 pA and analyzed the first supra-threshold event (Figure 5C).

Action potentials were characterized regarding their voltage and current thresholds, their height and their half-width (Figure 5D). None of these parameters displayed a clear correlation with the position of the cell within the LSO but differed between the two populations. Onset firing neurons had slightly higher voltage thresholds (-43.75 ± 3.39 mV vs. 38.89 ± 2.80 mV; $p = 0.12$) and significantly elevated current thresholds (0.72 ± 0.12 nA vs. 1.38 ± 0.17 nA; $p < 0.05$). Action potentials of continuously spiking cells were on average higher (90.87 ± 6.60 mV vs. 82.42 ± 1.94 mV; $p = 0.09$) and significantly broader (654.63 ± 106.76 μ s vs. 162.22 ± 76.17 μ s; $p < 0.0005$).

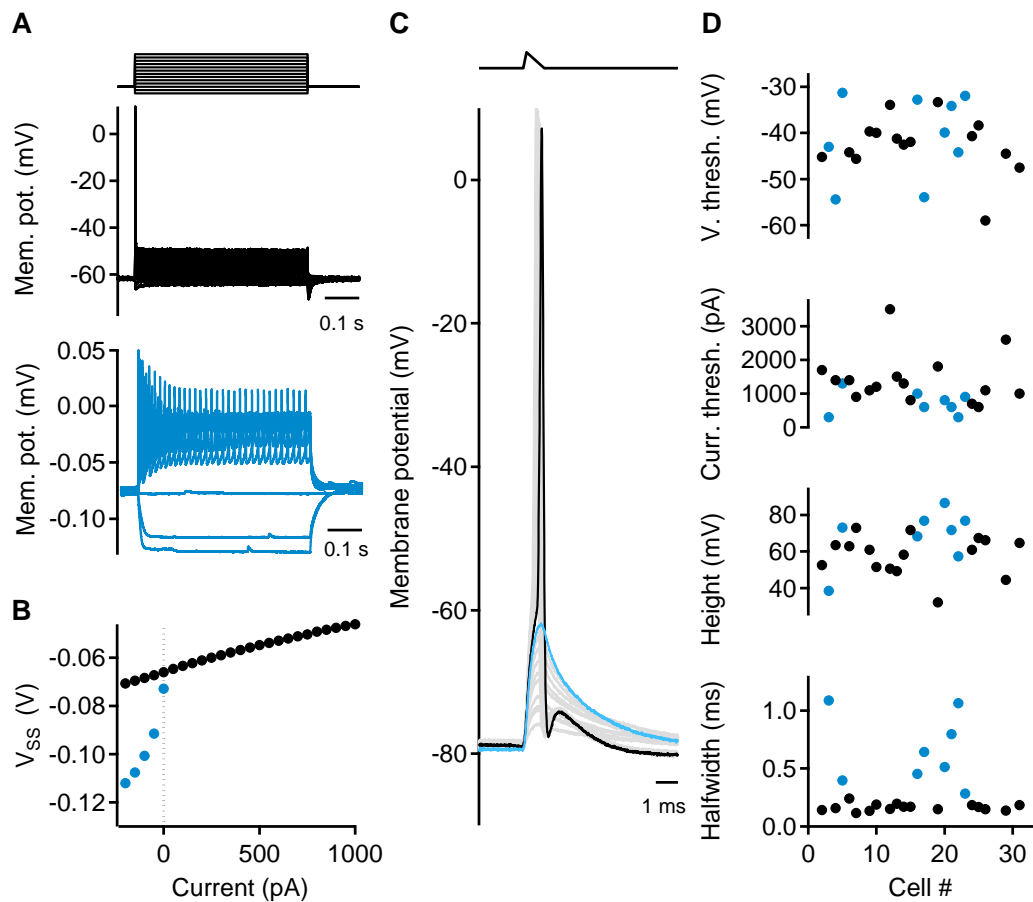


Figure 5: Firing patterns and action potentials in LSO neurons. **A:** Characterization of the firing behavior in response to 500 ms-long current injections between -200 and +1000 pA (top) revealed two types of firing patterns: cells firing an onset action potential (black, $n = 17$) and continuously spiking cells (blue, $n = 8$). **B:** steady state potentials as a function of the injected current for both cell types. **C:** Action potentials elicited by increasing stimuli approximating the shape of an EPSC. The last sub-threshold response is shown in blue. From the first suprathreshold event (black), the current and voltage thresholds, the height and the half-width were analyzed and plotted according to the cell's location in the LSO (**D**). Black dots indicate single-spiking cells, blue dots represent cells with repetitive firing ($n = 25$).

In summary, the LSO of mature mice is composed of at least two types of neurons with different intrinsic properties that differ in their input resistance, firing pattern and action potential characteristics. Onset spiking cells display a gradient in R_{in} that increases along the tonotopic axis of the LSO from medial to lateral.

Synaptic transmission in the mature LSO

The lateral superior olive integrates ipsilateral excitatory input with contralateral inhibitory input. To gain insight into synaptic transmission in the LSO, I studied the properties of spontaneous and evoked inhibitory and excitatory postsynaptic currents in the following set of experiments.

Figure 6A shows an example for the spontaneous synaptic activity recorded from a LSO neuron. Pharmacologically isolated miniature inhibitory or excitatory postsynaptic currents (mIPSCs and mEPSCs) were extracted and their amplitudes, decay time constants and frequencies were analyzed.

Figure 6B shows examples for the amplitude distribution of mEPSCs and mIPSCs in two cells. The inhibitory events had a slightly larger amplitude than mEPSCs (52.03 ± 9.62 pA vs. 34.60 ± 2.95 pA; $p = 0.08$) and decayed slower (1.06 ± 0.10 ms vs. 0.93 ± 0.15 ms; $p = 0.5$). With 8.91 ± 1.43 events per second, EPSCs occurred with a significantly higher frequency than IPSCs (4.74 ± 0.62 ; $p < 0.05$; Figure 6C).

To visualize possible differences along the tonotopic axis, the analyzed parameters were again arranged according to the cell's position in the LSO (Figure 6D).

Both mIPSCs and mEPSCs displayed no clear tendency from medial to lateral regarding their amplitudes and decay time constants. If anything, these parameters

showed a higher variability at more lateral positions. The frequency of mIPSCs was highest in medially located cells and decreased continuously. In the middle and lateral regions of the LSO, cells displayed either a rather high or low mEPSC frequency with increasing difference from medial to lateral.

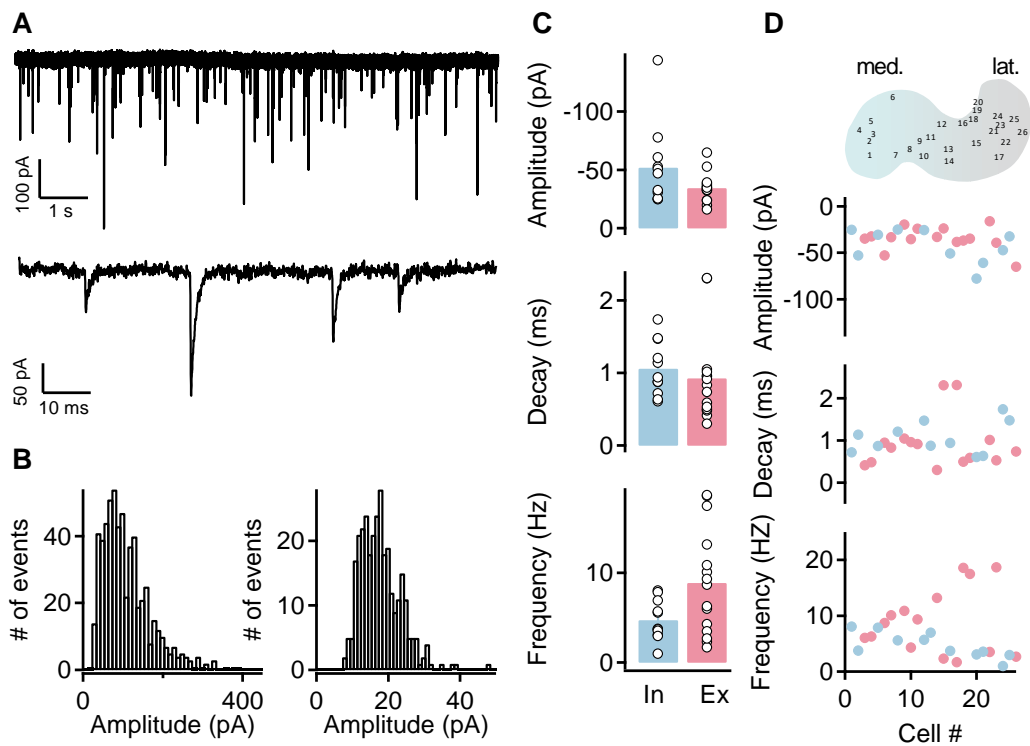


Figure 6: Miniature inhibitory and excitatory events in the LSO. **A:** Example recording of mIPSCs shown at low (top) and higher temporal resolution (bottom). **B:** Example amplitude distributions of mIPSCs (left) and mEPSCs. **C:** Average and individual results (circles) for the amplitudes, decay time constants and frequencies of inhibitory (blue) and excitatory (red) miniature events. **D:** mIPSC (blue) and mEPSC (red) amplitudes, decay time constants and frequencies of single cells plotted against the recording position along the LSO. mIPSCs: n = 11 cells / 4849 events; mEPSCs: n = 15 cells / 7070 events.

To analyze evoked postsynaptic currents, fibers projecting to the recorded neuron were stimulated by an electrode placed in the vicinity of the cell. Figure 7A shows examples for pharmacologically isolated excitatory (right) and inhibitory postsynaptic currents (left) evoked by various stimulation intensities (0 - 100 V) incremented in steps of 2 - 10 V.

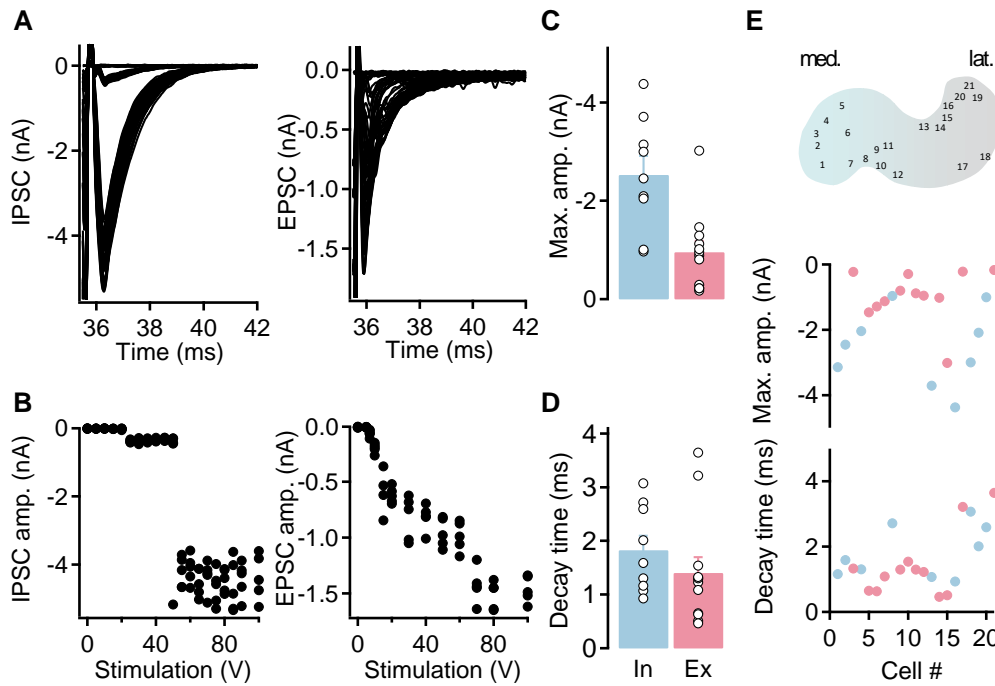


Figure 7: Evoked excitatory and inhibitory postsynaptic currents in LSO neurons. **A:** Example recordings of IPSCs (left) and EPSCs (right) evoked by stimulations of 0 – 100 V. **B:** IPSC (left) and EPSC amplitudes (right) as a function of the stimulation strength. **C, D:** Average maximal amplitudes (**C**) and decay time constants (**D**) of IPSCs (blue) and EPSCs (red). Circles represent individual cells. **E:** Maximal amplitudes and decay times of IPSCs (blue) and EPSCs (red) arranged according to the position of the cell in the LSO. EPSCs: n = 9; IPSCs: n = 12.

The peak amplitudes were dependent on the stimulation strength and usually increased rather stepwise than gradually (Figure 7B), which is generally interpreted as the recruitment of additional fibers projecting to the neuron.

IPSCs had a significantly larger maximal amplitude than EPSCs (2.53 ± 0.38 nA vs. 0.96 ± 0.23 nA; $p < 0.005$; Figure 7C) and a slightly slower decay time of 1.83 ± 0.27 ms than the excitatory currents (1.41 ± 0.29 ms; $p = 0.32$; Figure 7D).

With correlation coefficients of 0.03 (IPSCs) and -0.18 (EPSCs), the amplitudes of evoked postsynaptic currents showed no clear relation with the position of the neuron along the tonotopic axis (Figure 7E; top graph). In contrast, excitatory and inhibitory currents displayed a tendency to slower decay time constants in cells recorded at the lateral edge of the LSO compared to cells located more medially (IPSCs: $p = 0.57$; EPSCs: $p = 0.39$; Figure 7E, bottom).

Taken together, this study provides a characterization of the basic intrinsic properties of neurons in the mature LSO and their inhibitory and excitatory synaptic inputs. In addition, the results indicate that the position of a neuron along the tonotopic axis of the LSO is reflected in adaptations of some of the intrinsic and synaptic properties.

3. CONSEQUENCES OF TWO DEAFNESS-RELATED MUTATIONS FOR A LARGE CENTRAL AUDITORY SYNAPSE

The previous experiments provided a characterization of the cellular and synaptic properties in an auditory brainstem nucleus of normal-hearing mice. To understand the mechanisms underlying normal development and function of the auditory system, the study of deafness-related changes can provide additional insight. In this study I compared two mutations that have been shown to cause hearing disorders in both mice and humans: the *Diminuendo* mouse, in which the mutation affects the peripheral and the central nervous system, and the Claudin-14-knockout mouse, where the defect is only peripheral.

The *Diminuendo* (*dmdo/dmdo*) mutation is a single base change in the seed region of microRNA-96. MicroRNAs are small non-coding RNAs involved in the regulation of posttranscriptional gene expression by binding to complementary sites on their target mRNAs. MicroRNA-96 is expressed in the mammalian cochlear and has been shown to play a crucial role in coordinating the development and maturation of the peripheral auditory system. Mutations are associated with hearing loss in mice (Lewis et al., 2009) and humans (Mencia et al., 2009) and lead to a physiological and morphological arrest in cochlear hair cell differentiation around the day of birth in homozygous mice (Lewis et al., 2009; Kuhn et al., 2011). Quantitative RT-PCR analysis recently demonstrated that miR-96 is also expressed in the auditory brainstem and up-regulated during development (Rosengauer et al., 2012), suggesting that this miRNA plays a role in the maturation process of the central auditory system as well.

The Claudin-14^{-/-} mouse is a model for peripheral hearing loss only and hence contrasts the peripheral and central deficiencies in the *Diminuendo* mouse. Claudin-14 is a tight junction protein that is required in the reticular lamina to form a cation-restrictive barrier. Its absence leads to a failure in maintaining the cochlear fluid compartmentalization, resulting in the rapid death of outer hair cells, followed by slower degeneration of inner hair cells during the first three weeks of life in mice (Ben-Yosef et al., 2003).

The comparison of these two mouse models should allow to separate central changes induced by the *Diminuendo* mutation from alterations that are a result of peripheral hair cell deficiencies in the auditory brainstem.

In the following, I analyzed the morphological and functional consequences of these mutations in homozygous animals and their respective wildtype. Experiments were performed in the medial nucleus of the trapezoid body, a rather homogenous brainstem nucleus that represents the first inhibitory hub in auditory processing and acts mainly as a relay. MNTB principal neurons are innervated by single large glutamatergic terminals that form the calyx of Held, a giant synapse that has become an established model for detailed structural and functional studies of signal transmission in the auditory brainstem (Nakamura and Cramer, 2011) and that exhibits little activity-dependent plasticity (Oleskevich et al., 2004; Youssoufian et al., 2005; Youssoufian et al., 2008). Therefore, the MNTB is well-suited to investigate the intrinsic and synaptic effects of these hearing disorders.

To reduce possible influences of the tonotopic gradient in neuronal properties (Li et al., 2001; Barnes-Davies et al., 2004; von Hehn et al., 2004; Brew and Forsythe, 2005), all neurons were recorded from the middle third of the MNTB.

Morphology

In order to investigate whether these mutations lead to morphological alterations of the pre- and postsynaptic compartments of the MNTB, immunostainings for MAP2 for somata and SV2 as a presynaptic marker were applied (Figure 8A). *Dmdo/dmdo* mice showed a significant decrease in cell diameter ($16.40 \pm 0.29 \mu\text{m}$) compared to their wildtype littermates ($18.15 \pm 0.21 \mu\text{m}$; $p < 0.0005$) whereas the size of neurons in *Cldn-14^{-/-}* mice did not differ from the control group (17.51 ± 0.44 vs. $17.13 \pm 0.64 \mu\text{m}$; $p = 0.63$; Figure 8B).

Figure 8C (left) shows example stainings of presynaptic terminals surrounding *Diminuendo* wildtype and mutant MNTB neurons and average images of the donut-like substructures for each group (Figure 8C, middle and right). To quantify the apparent morphologic changes at the calyx of Held, the grey value of individual donuts was determined by line scans and normalized over the dynamic range (Figure 8D). Donuts in *Diminuendo* wildtype mice were rather uniform and showed a well-defined round shape, leading to lower signal intensities distant to the center. In *dmdo/dmdo* mice these structures appeared distorted and accordingly, the average signal intensity was higher at the edges. In *Cldn-14^{-/-}* and control animals, the donuts seemed less defined compared to *Diminuendo* wildtypes.

In contrast to the *Cldn-14^{-/-}* and *Cldn-14^{+/+}* mice, both the calyces of Held and the postsynaptic neurons in *dmdo/dmdo* mice were clearly different from the control, indicating that these alterations originate in the brainstem and are not a consequence of peripheral defects.

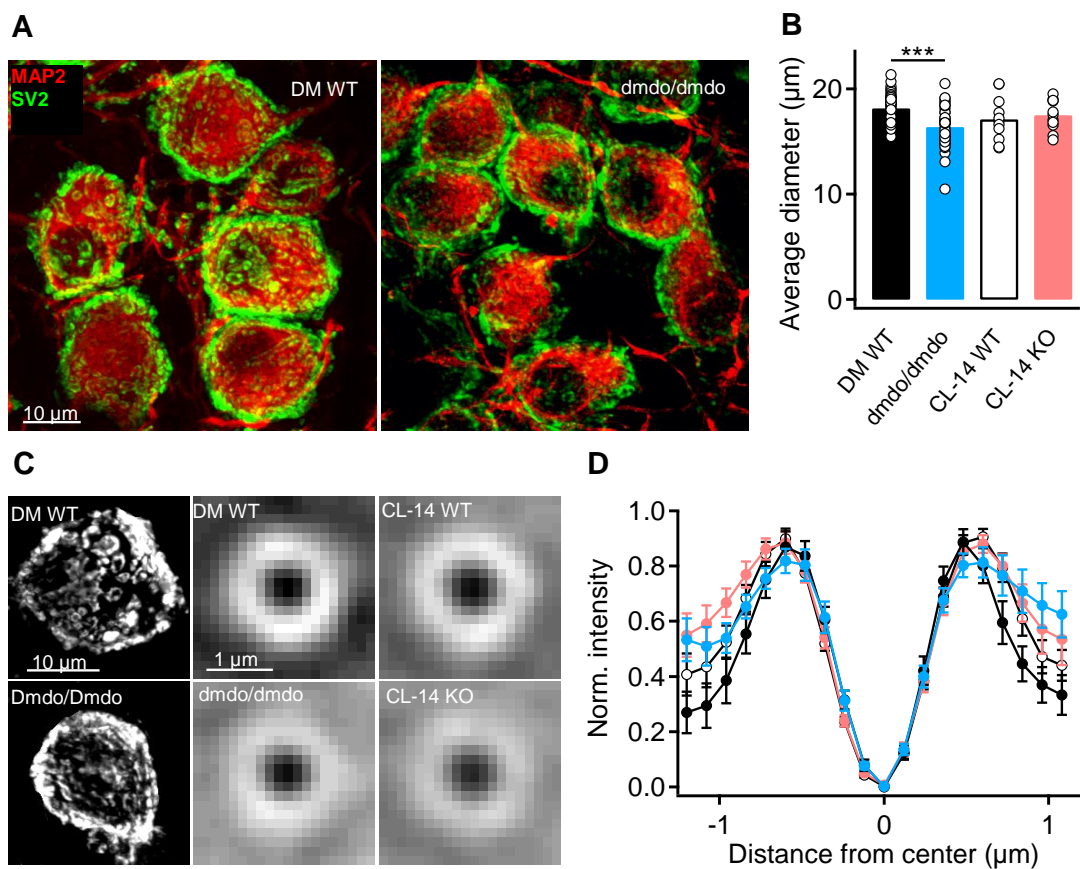


Figure 8: Pre- and postsynaptic morphology in the MNTB. **A:** Immunostainings against MAP2 (red) and SV2 (green) as markers for somata and presynaptic terminals in the MNTB of *Diminuendo* (DM) wildtype (left) and mutant animals (right). **B:** Average soma diameter of MNTB principal neurons in DM WT (n = 42), *dmdo/dmdo* (n = 42), Claudin-14 (CL-14) wildtype (n = 11) and CL-14 KO (n = 11). Circles represent single cells. **C** (left): Example SV2 stainings of the presynaptic structures surrounding a neuron in DM WT (top) and mutant mice (bottom). Middle and right: Average images of all extracted donuts scaled to the same signal intensity (DM WT: n = 278 donuts/ 12 cells; *dmdo/dmdo*: n = 281 donuts, 12 cells; CL-14 WT: n = 231 donuts, 11 cells; CL-14 KO: n = 275 donuts, 11 cells). **D:** Averaged signal intensity of the donuts determined by line scans and normalized over the dynamic range.

Passive properties

To study whether these alterations in cell morphology are also accompanied by functional changes, I first estimated the passive membrane properties of MNTB neurons. Parameters like the input resistance R_{in} , the membrane time constant τ_m and the cell capacitance C_m influence the integration of synaptic inputs and interact with active properties, hence contributing to voltage signaling in the MNTB.

These parameters were analyzed from the average voltage response to 200 ms-long current injections of -5 pA (Figure 9A) and from the average response to a 10 mV hyperpolarization from a holding potential of -60 mV (Figure 9E). The current and voltage steps were kept small to minimize the activation or deactivation of additional voltage-dependent conductances, hence the passive properties can be estimated (Ammer et al., 2012; Berger et al., 2014; Franzen et al., 2015). Both paradigms allow for the calculation of R_{in} according to Ohm's Law which then in turn can be used to estimate the cell capacitance ($C_m = \tau / R_{in}$).

Under current-clamp conditions, neurons in *dmdo/dmdo* mice showed a slightly elevated R_{in} ($279.13 \pm 43.77 \text{ M}\Omega$) compared to their wildtype littermates ($235.91 \pm 44.46 \text{ M}\Omega$, $p = 0.50$). A similar difference in R_{in} was calculated for *Cldn-14^{-/-}* and control mice (273.38 ± 56.46 and $231.53 \pm 44.46 \text{ M}\Omega$, respectively; $p = 0.57$; Figure 9B). The values for R_{in} obtained from the voltage-clamp paradigm were generally lower, however the trend between the four groups remained comparable (DM WT: $176.78 \pm 26.14 \text{ M}\Omega$, *dmdo/dmdo*: $267.76 \pm 63.64 \text{ M}\Omega$, $p = 0.22$; *Cldn-14^{-/-}*: $266.27 \pm 62.70 \text{ M}\Omega$, *Cldn-14^{+/+}*: $176.78 \pm 26.143 \text{ M}\Omega$, $p = 0.42$; Figure 9F).

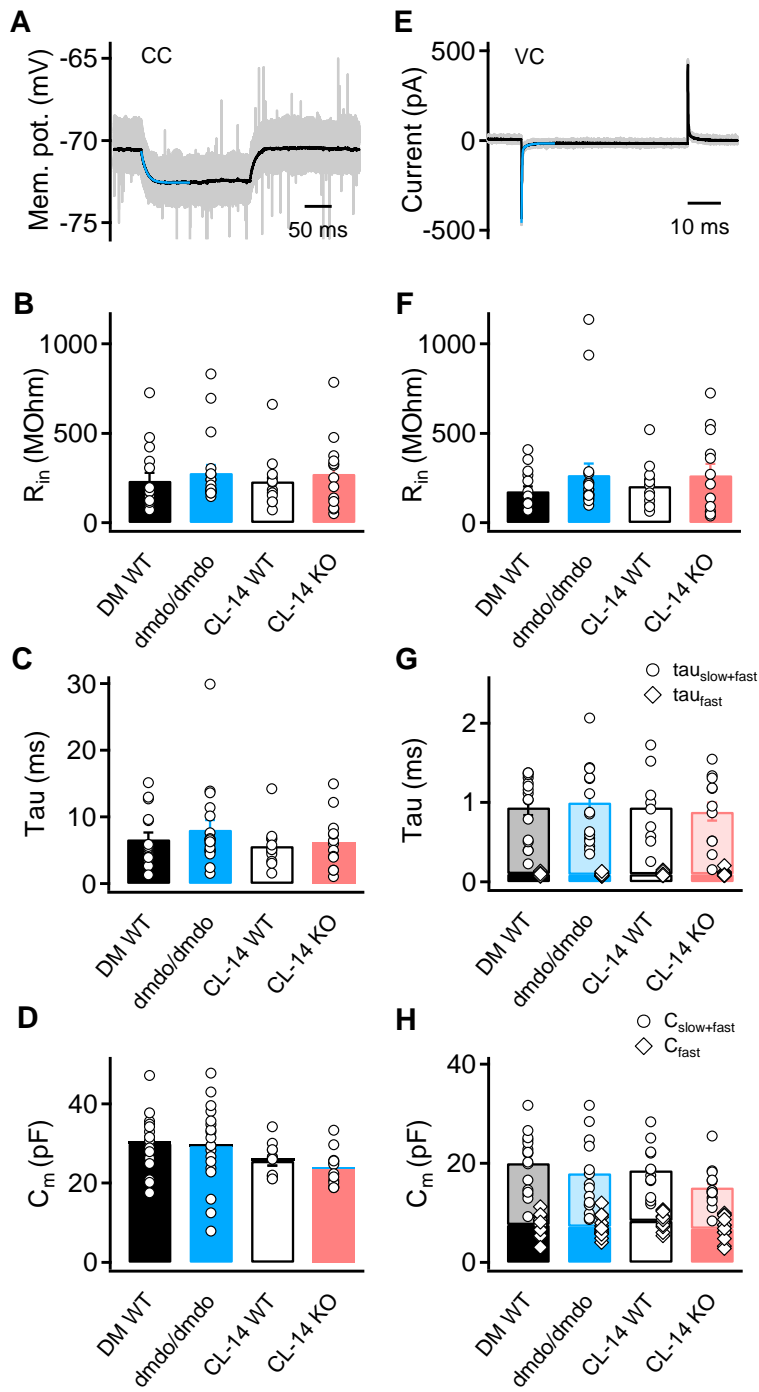


Figure 9: Passive membrane properties of MNTB neurons. A: Voltage responses to 200 ms-long current injections of -10 pA. The average potential (black) was calculated from 60 trials (grey) and an exponential function (blue) was fitted to the onset of the response. This

protocol was used to estimate R_{in} (B), τ (C) and C_m (D) in current-clamp conditions. Circles represent values for individual cells. E: 50 single trials (grey) and the average current (black) induced by 10 mV hyperpolarizations, fitted with a double exponential function (blue). F: Average R_{in} calculated from the voltage-clamp protocol and individual values shown as circles. The double-exponential fit results in a fast and a slow component of τ (G) and accordingly, lead to two different values for C_m , representing the slow and the fast charging compartment (H). Bottom parts of the bars and rectangular symbols correspond to values based on τ_{fast} , entire bars and circles represent $\tau_{fast} + \tau_{slow}$ and the corresponding values for C_m . DM WT: n = 16, *dmdo/dmdo*: n = 19, CL-14 WT: n = 12, CL-14 KO: n = 13.

Membrane time constants were extracted from mono- (Figure 9A) or bi-exponential functions (Figure 9E) fitted to the onset of the average voltage or current responses. Figure 9C shows a slightly faster τ for *Cldn-14^{-/-}* and control mice (*Cldn-14^{-/-}*: 6.21 ± 1.11 ms, *Cldn-14^{+/+}*: 5.67 ± 0.91 ms, $p = 0.71$) compared to *Diminuendo* mutants and wildtypes (*dmdo/dmdo*: 8.09 ± 1.43 ms, DM WT: 6.67 ± 1.01 ms, $p = 0.44$), resulting in a marginally smaller C_m in the Claudin-14 group (DM WT: 30.06 ± 1.85 pF, *dmdo/dmdo*: 29.42 ± 2.31 pF, $p = 0.83$; *Cldn-14^{+/+}*: 25.62 ± 1.21 pF, *Cldn-14^{-/-}*: 23.52 ± 1.23 pF, $p = 0.23$; Figure 9D).

The current deflection in voltage clamp mode shown in Figure 9B could be better described by a bi-exponential function, leading to membrane time constants with a fast and a slow component (Figure 9G) and hence, to two estimated capacitances corresponding to τ_{fast} and τ_{slow} (Figure 9H). Neither τ_{fast} (DM WT: 0.101 ± 0.005 ms, *dmdo/dmdo*: 0.090 ± 0.004 ms, $p = 0.11$; *Cldn-14^{+/+}*: 0.099 ± 0.007 ms, *Cldn-14^{-/-}*: 0.100 ± 0.010 ms, $p = 0.93$) nor τ_{slow} (DM WT: 0.839 ± 0.100 ms, *dmdo/dmdo*: 0.911 ± 0.111 ms, $p = 0.64$; *Cldn-14^{+/+}*: 0.840 ± 0.125 ms, *Cldn-14^{-/-}*: 0.784 ± 0.112 ms, $p = 0.74$; Figure 9G) showed significant differences between the four groups.

The total electronically effective capacitance calculated from R_{in} and τ was slightly, but not significantly larger in the control groups (DM WT: 20.04 ± 1.51 pF, *dmdo/dmdo*: 16.80 ± 1.87 pF, $p = 0.18$; *Cldn-14^{+/+}*: 18.61 ± 1.47 pF, *Cldn-14^{-/-}*: 15.16 ± 1.16 pF, $p = 0.07$). The capacitance corresponding to the fast component of τ was 7.59 ± 0.50 pF in DM WT, 7.24 ± 0.45 pF in *dmdo/dmdo* ($p = 0.60$), 8.41 ± 0.49 pF in *Cldn-14^{+/+}* and 6.82 ± 0.64 in *Cldn-14^{-/-}* mice ($p = 0.06$; Figure 9H).

Taken together, neither a peripheral hearing loss nor the mutation of miR-96 seem to alter the passive membrane parameters of MNTB neurons considerably, since both paradigms could not show any significant effects on the input resistance, the membrane time constant and the capacitance. To find out whether the active properties remain unaffected by these mutations as well, I next analyzed the firing behavior and action potential properties in MNTB neurons.

Active properties and firing behavior

The firing behavior of MNTB principal neurons was characterized in response to 300 ms-long current injections, incremented in 100 pA steps from -200 to -1000 pA. Neurons in all four groups responded either with one or a few onset spikes (Figure 10A) or they showed a sustained firing pattern (Figure 10B). In *Cldn-14^{-/-}* and wildtype mice, the proportion of both firing types seemed comparable: 8 of 13 cells in the wildtype and 7 of 13 cells in the knockout responded with onset spikes. In the *Diminuendo* control group, the onset firing pattern clearly predominated (10 of 16 cells) while in the mutants, two-thirds of neurons fired continuously (Figure 10E).

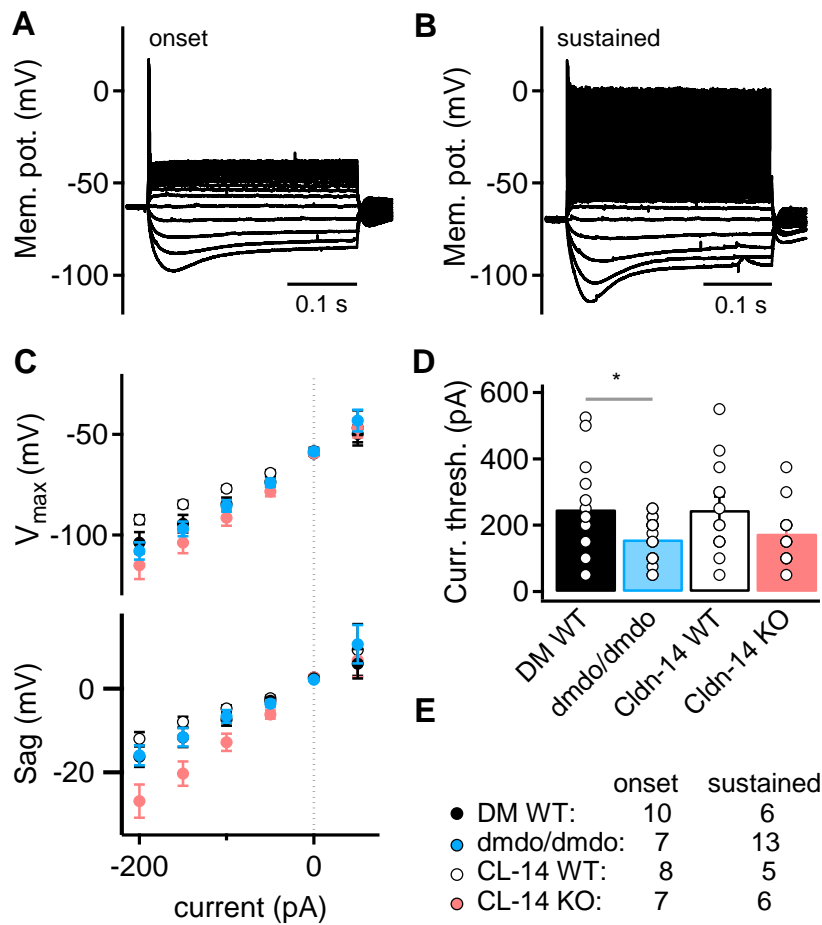


Figure 10: Firing behavior of MNTB neurons. **A, B:** MNTB neurons showed either an onset action potential (**A**) or a sustained firing pattern (**B**) in response to 300 ms-long current injections of -200 to +1000 pA. **C:** the maximal current amplitude (top Graph) and the sag potential (bottom) plotted against the injected current. **D:** Bars represent average current thresholds, single cells are indicated by open circles. **E:** numbers for onset and sustained firing neurons in the different groups.

Average current thresholds in *dmdo/dmdo* and *Cldn-14^{-/-}* neurons were reduced compared to their respective controls and in *dmdo/dmdo* mice, this reduction was significant (DM WT: 248.44 ± 32.39 pA, *dmdo/dmdo*: 157.50 ± 14.41 pA, $p < 0.05$; *Cldn-14^{+/+}*: 246.15 ± 39.11 pA, *Cldn-14^{-/-}*: 175.00 ± 24.35 pA, $p = 0.14$; Figure 10D). V_{\min} did not differ between *dmdo/dmdo* neurons and their controls while in the Claudin-14 group, wildtype neurons displayed a larger voltage deflection compared to the knockout (Figure 10C, top). The sag potential, measured by subtracting the steady-state potential from the hyperpolarization minimum, was also similar in *Diminuendo* mutant and wildtype cells, whereas *Cldn-14^{-/-}* neurons had a larger sag than their wildtype counterparts (Figure 10C, bottom).

To analyze the characteristics of a single action potential in detail, I used a stimulus that approximates the shape of an EPSC and is therefore physiologically more relevant than prolonged depolarizations (Franzen et al., 2015). Currents with a rise time of 0.2 ms and a decay time of 0.45 ms and were incremented in steps of 100 pA and action potential parameters were analyzed from the first supra-threshold event (Figure 11A).

The average current thresholds were noticeably reduced in *dmdo/dmdo* neurons compared to their wildtypes while *Cldn-14^{-/-}* mice showed no such difference (*dmdo/dmdo*: 1.67 ± 0.13 nA, DM WT: 2.10 ± 0.19 nA; $p = 0.067$; *Cldn-14^{+/+}*: 1.82 ± 0.18 nA, *Cldn-14^{-/-}*: 1.69 ± 0.24 nA, $p = 0.67$; Figure 11E). The other parameters investigated did not differ between normal hearing and mutant animals. The duration of the action potential, determined as the half-width measured from resting potential, did not differ significantly between the four groups (DM WT: 281.16 ± 14.59 μ s, *dmdo/dmdo*: 249.82 ± 13.66 μ s, $p = 0.95$; *Cldn-14^{+/+}*: 260.79 ± 25.20 μ s, *Cldn-14^{-/-}*: 277.16 ± 23.44 μ s, $p = 0.37$; Figure 11B). The peak of the first supra-threshold response was reached after 1.15 ± 0.07 ms in DM WT, 1.04 ± 0.08 ms in *dmdo/dmdo* ($p = 0.07$), 1.33 ± 0.11 ms in *Cldn-14^{+/+}* and 1.27 ± 0.14 ms in *Cldn-14^{-/-}* ($p = 0.67$; Figure 11F).

Interestingly, the study revealed considerable strain-specific differences between the NMRI mice used for the Claudin-14 knockout and the C3HeB/FeJ line that served as background for the *Diminuendo* group. Action potentials were significantly higher in C3HeB/FeJ (DM WT: 53.14 ± 4.03 mV, *dmdo/dmdo*: 53.61 ± 4.07 mV, *Cldn-14^{+/+}*: 35.12 ± 5.92 mV, *Cldn-14^{-/-}*: 33.49 ± 4.58 mV, $p < 0.05$ when comparing both wildtypes; Figure 11C) and showed significantly elevated voltage thresholds (DM WT: -37.90 ± 3.45 mV, *Cldn-14^{+/+}*: -19.90 ± 4.87 mV, $p < 0.005$; *dmdo/dmdo*: -38.20 ± 3.54 mV, *Cldn-14^{-/-}*: -19.30 ± 4.43 mV; Figure 11D).

In summary, the analysis of the active properties of MNTB principal neurons demonstrated several differences between the four groups. Reduced current thresholds were observed for both hearing-deficient mice, although more prominent in *dmdo/dmdo* animals, and possibly compensate for the lack of normal synaptic activity to maintain the overall excitability in the circuit. The large proportion of neurons that display sustained firing in *dmdo/dmdo* mutant mice could hint to a specific effect of miR-96 on intrinsic properties of auditory brainstem neurons.

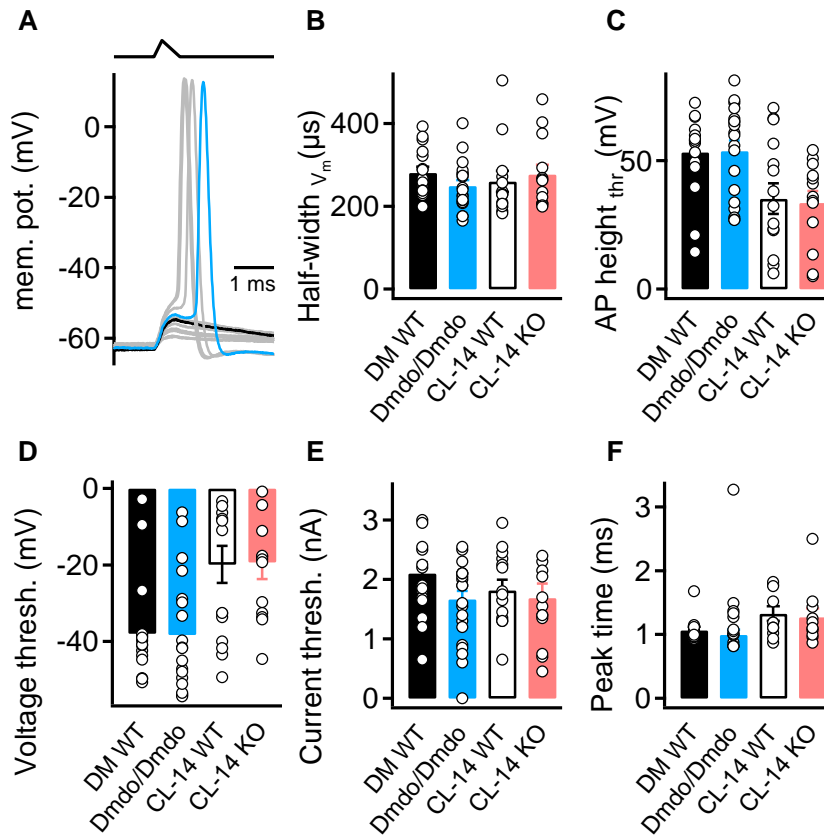


Figure 11: Action potential properties. **A:** Action potentials elicited by an EPSC-approximating stimulus (top) incremented in 100 pA steps. The last sub-threshold event is shown in black, and from the first action potential (blue), the half-width (**B**), the height (**C**), the voltage- (**D**) and current thresholds (**E**) and the time to peak (**F**) were analyzed. Circles represent individual cells. DM WT: $n = 16$, *dmdo/dmdo*: $n = 19$, CL-14 WT: $n = 13$, CL-14 KO: $n = 13$.

Miniature EPSCs

Figure 8 showed alterations of the presynaptic substructures that form the calyx of Held in *dmdo/dmdo* mutants as well as differences between the two mouse lines. To probe for accompanying changes in synaptic transmission, pharmacologically isolated miniature excitatory postsynaptic currents (mEPSCs) were quantified. Only cells with more than 40 mEPSCs and with recordings of at least 180 s duration were included.

Figure 12A (top) shows an example trace and the corresponding histogram of the amplitude distribution (bottom left). The decay time constant was obtained from an exponential function fitted to the average mEPSC (bottom right).

With 85.96 ± 6.59 pA, mEPSCs in *dmdo/dmdo* mutant mice had a significantly higher median amplitude compared to their wildtype littermates (66.71 ± 4.47 pA; $p < 0.05$). The *Cldn-14^{-/-}* animals also showed a slight increase in amplitude compared to their normal hearing counterparts (*Cldn14^{-/-}*: 60.68 ± 6.26 pA, *Cldn-14^{+/+}*: 44.16 ± 7.91 pA, $p = 0.13$; Figure 12B).

In the *Diminuendo* group, 5.58 ± 1.11 (*dmdo/dmdo*) and 4.88 ± 0.99 (WT) mEPSCs per second were detected on average ($p = 0.64$). The mEPSC frequency in Claudin-14 wildtype mice was with 3.33 ± 1.71 events per second slightly lower than in the mutants (5.98 ± 1.88 mEPSCs/s, $p = 0.24$; Figure 12C).

To characterize the kinetics of the miniature postsynaptic currents, the 20 – 80 % rise time and the decay time constant were analyzed from the average mEPSC of each cell. Miniature EPSCs in the *Diminuendo* group displayed no significant differences between normal hearing and mutant mice regarding their rise time (DM WT: 83.5 ± 2.7 μ s; *dmdo/dmdo*: 77.8 ± 1.9 μ s, $p = 0.10$). Also for knockout and wildtype animals in the Claudin-14 group, no changes in rise time were detected

(Cldn-14^{-/-}: $90.2 \pm 3.4 \mu\text{s}$; Cldn-14^{+/+}: $90.3 \pm 2.7 \mu\text{s}$, $p = 0.15$; Figure 12D). The decay time constants determined from single exponential functions were $0.18 \pm 0.02 \text{ ms}$ (DM WT), $0.17 \pm 0.01 \text{ ms}$ (dmdo/dmdo; $p = 0.49$), $0.23 \pm 0.02 \text{ ms}$ (Cldn-14^{+/+}) and $0.19 \pm 0.02 \text{ ms}$ (Cldn-14^{-/-}; $p = 0.18$; Figure 12E).

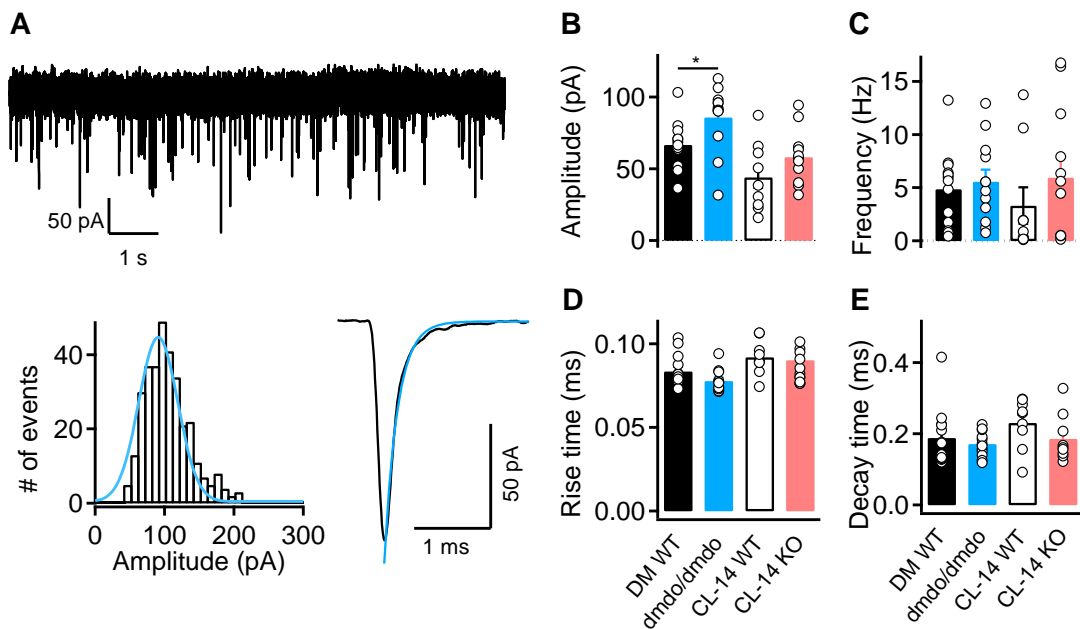


Figure 12: Miniature EPSCs in the MNTB. **A:** Example recording of mEPSCs (top) and the amplitude distribution of all detected events (bottom left). The decay time constant was extracted from an exponential fit (blue) to the average mEPSC (bottom right). For each cell, the median amplitude (**B**), frequency (**C**), rise time (**D**) and decay time (**E**) were characterized. DM WT: $n = 13$, dmdo/dmdo: $n = 12$, CL-14 WT: $n = 9$, CL-14 KO: $n = 9$.

The significantly increased mEPSC amplitude in *Diminuendo* mutant mice, together with a slightly elevated frequency suggests a possible effect of miR-96 on synaptic transmission in the auditory brainstem. To investigate this question further, I studied EPSCs evoked by stimulation trains of different frequencies in the following experiments.

Evoked EPSCs

To evoke EPSCs, a bipolar stimulation electrode was placed in the fibers between the midline and the MNTB. The stimulus strength was adjusted to reliably produce an EPSC in response to each pulse. Inputs were stimulated with trains of 20 pulses at 10, 20, 50, 100, 300 and 500 Hz and the average current of four repetitions for each frequency was analyzed.

In all four groups, I found neurons with two different types of inputs. Figure 13A shows an example for a large input from a calyx terminal that is characterized by a high initial EPSC amplitude and displayed depression at higher stimulation frequencies. In contrast, the EPSCs of the smaller non-calyceal inputs shown in Figure 13B often facilitated. The proportion of large and small inputs in the different groups is presented in Figure 13J.

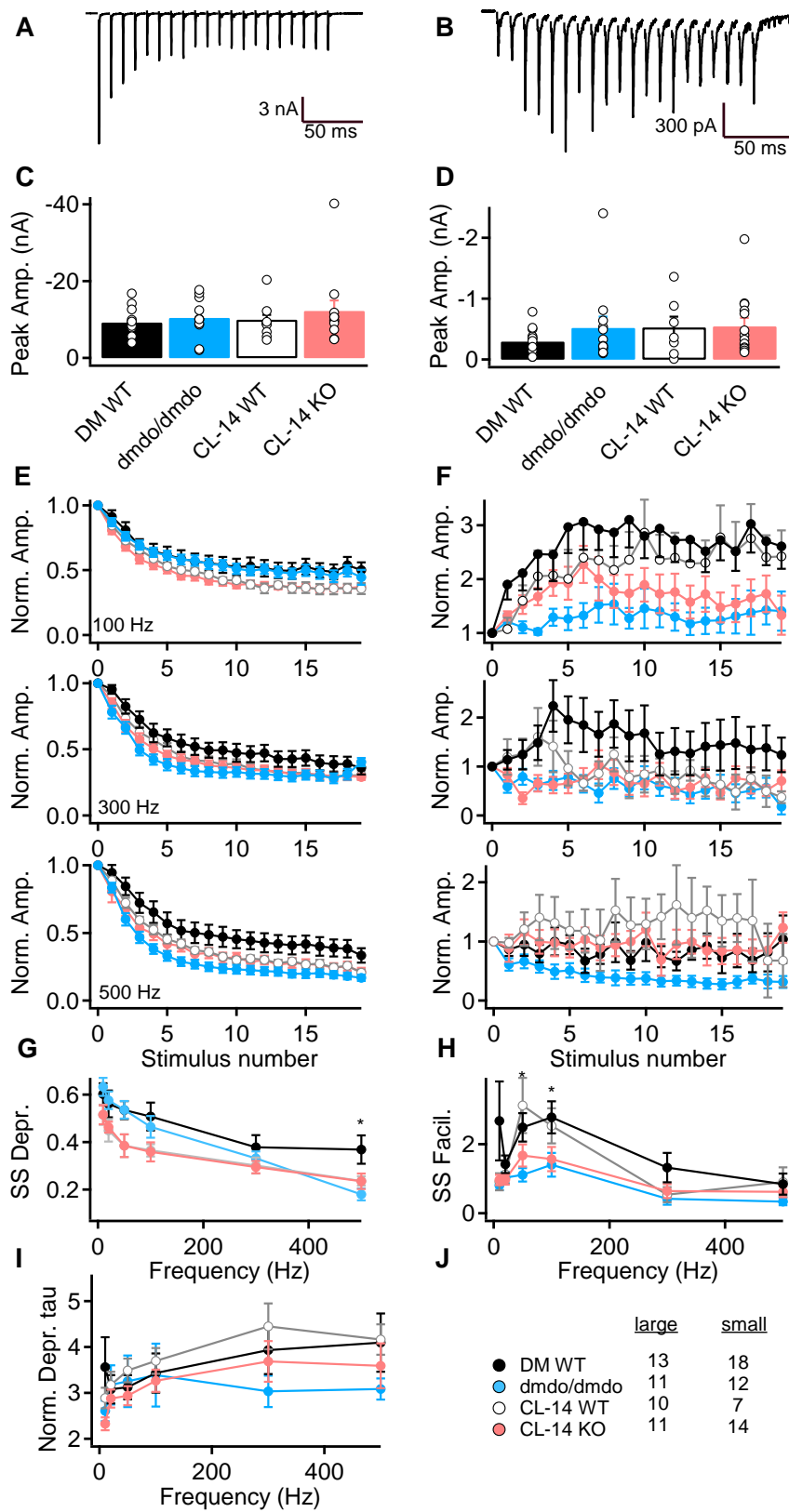


Figure 13: Characterization of large and small inputs. **A, B:** example responses to train stimulations of MNTB neurons receiving large calyceal inputs (**A**) and small inputs (**B**). **C, D:** Average peak amplitudes for large (**C**) and small inputs (**D**). Circles represent values for individual cells. **E, F:** Normalized EPSC amplitudes as a function of the pulse number for large (**E**) and small inputs (**F**) for stimulation frequencies of 100, 300 and 500 Hz. **G:** Steady state depression as a function of the stimulation frequency for cells receiving a calyceal input. **H:** Facilitation observed in cells receiving small inputs as a function of the stimulation frequency. **I:** Time constants of the depression plotted for each stimulation frequency. **J:** Proportion of neurons receiving large and small inputs.

The average amplitudes of the first EPSC were not significantly altered by the mutations. Large inputs in *Diminuendo* wildtype neurons had a peak current of 9.27 ± 0.99 nA compared to 10.90 ± 1.43 nA in the mutant ($p = 0.52$). The peak amplitudes for Claudin-14 wildtype and knockout animals were 9.27 ± 0.90 and 12.29 ± 2.69 nA, respectively ($p = 0.45$; Figure 13C). Stimulating the small inputs lead to EPSCs with average amplitudes of 298.31 ± 47.82 pA in *Diminuendo* wildtype neurons, 519.68 ± 18.33 pA in the mutant ($p = 0.19$), 513.39 ± 10.81 pA in the Claudin-14 control and 552.26 ± 13.44 pA in the knockout ($p = 0.67$; Figure 13D).

Figure 13E illustrates the depression of large EPSC amplitudes from the first to the last pulse. The depression was dependent on the frequency and stronger in *dmdo/dmdo* animals. At 100 Hz, the amplitude decreased to 50% of its initial value in the *Diminuendo* control and to 44 % in the mutant. At 500 Hz, the amplitude of *dmdo/dmdo* mice was reduced to 17 % compared to 33 % in the wildtype. In contrast, the depression of EPSCs in Claudin-14 wildtype and knockout mice remained similar. Figure 13G summarizes the depression of EPSCs for all frequencies used by plotting the average depression of the last three normalized

EPSCs against the frequency. Claudin-14^{+/+} and knockout mice displayed a nearly identical course. In *Diminuendo* mutants, the amplitude continued to decrease with increasing frequency while in the wildtype, the depression reached a plateau. At 500 Hz, the difference between both groups was significant ($p < 0.05$).

To extract the time course of the depression for each frequency, an exponential function was fitted to the amplitudes of the 20 EPSCs of each cell (Figure 13). The *dmdo/dmdo* mutant cells exhibited the fastest depression of all groups for frequencies above 100 Hz. In *Cldn-14*^{-/-} mice, the decrease in amplitude occurred faster compared to their wildtype littermates as well.

EPSCs evoked by stimulation of the small inputs showed facilitation as exemplified in Figure 13F for 100, 300 and 500 Hz and plotted in Figure 13H for all frequencies. In general, the facilitation was most pronounced at low-frequency stimulations and in the control groups. Again, there was a clear difference between *dmdo/dmdo* mice and their wildtype counterparts that was most significant at stimulation frequencies of 50 and 100 Hz ($p < 0.05$ in both cases). In contrast to the wildtype control, EPSCs of *Diminuendo* mutants showed only little or no facilitation. A similar trend was observed in Claudin-14 mice with lower facilitation in the hearing-deficient animals.

The cumulative EPSC (EPSC_{cum}) that may be used to compare the physiologically relevant apparent pool size (Elmqvist and Quastel, 1965) was calculated for three different stimulation frequencies in cells that received large inputs (Figure 14A). After an initial phase with a higher increase, the cumulative EPSC amplitude showed a linear rise during the later pulses. At 100 Hz, the EPSC_{cum} amplitude of *dmdo/dmdo* mice reached -121.90 ± 21.39 nA at pulse 20. At 300 and 500 Hz, the maximal amplitude was slightly reduced to -88.71 ± 18.48 nA ($p = 0.36$) and -69.48 ± 10.97 nA ($p = 0.16$ when compared to 100 Hz) respectively, suggesting a depletion

of the pool at higher frequencies. EPSC_{cum} amplitudes in *Diminuendo* control mice decreased less with higher stimulation frequencies (-99.63 ± 9.73 nA (100 Hz), -96.69 ± 10.25 nA (300 Hz; p = 0.98), -86.62 ± 9.91 (500 Hz; p = 0.65 when compared to 100 Hz at pulse 20)). The larger EPSC_{cum} at 500 Hz (p = 0.69 when comparing *dmdo/dmdo* and wildtype animals), together with the steeper slope, may indicate that wildtype synapses can transmit higher frequencies over longer periods of time. In the Claudin-14 group, the EPSC_{cum} in mutant mice reaches a slightly higher maximal amplitude at all stimulation frequencies than their normal-hearing littermates (*Cldn-14^{-/-}*: -103.02 ± 18.92 nA (100 Hz), -99.86 ± 15.93 nA (300 Hz), -81.84 ± 12.61 nA (500 Hz); *Cldn-14^{+/+}*: -81.82 ± 9.53 nA (100 Hz; p = 0.31), -87.66 ± 10.15 nA (300 Hz; p = 0.54), -73.17 ± 10.03 nA (500 Hz; p = 0.29 when compared to the knockout)).

Figure 14B shows the EPSC amplitudes plotted against EPSC_{cum} that allows for a linear extrapolation to the first EPSCs in a train of 20 stimuli. Based on the assumption that the EPSC size is proportional to the number of remaining quanta, the intersection with the x-axis provides an estimate of the releasable quanta (Elmqvist and Quastel, 1965; Taschenberger et al., 2002). This estimate was proportional to -67.43 nA (100 Hz), -81.16 nA (300 Hz) and -72.84 nA (500 Hz) in *Diminuendo* control mice. In the mutants, this value continually decreased with increasing stimulation frequency from -92.54 nA to -52.99 nA and -48.91 nA. In the Claudin-14 group, this analysis revealed no apparent differences between wildtype (-58.70 nA, -64.66 nA and -55.07 nA) and knockout mice (-60.87 nA, 62.67 nA and 56.51 nA for 100, 300 and 500 Hz, respectively).

These results indicate that deafness alone is not sufficient to alter the degree of depression at higher stimulation frequencies at the calyx of Held, suggesting that the observed changes in the *Diminuendo* mouse could be caused by the miR-96 mutation.

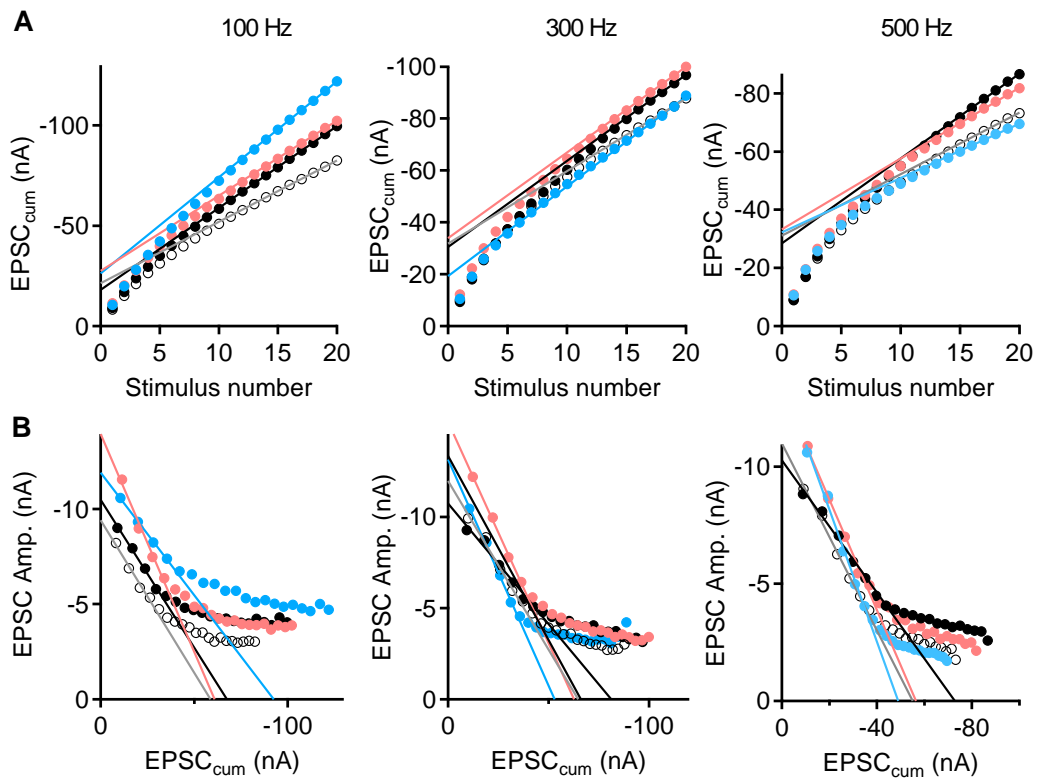


Figure 14: Cumulative EPSCs. **A:** cumulative EPSC amplitudes in DM WT (black), dmdo/dmmdo (blue), CL-14 WT (white) and CL-14 KO (red) for train stimulations with 100, 300 and 500 Hz. **B:** Plot of EPSCs versus the cumulative EPSC. Linear fits to the first four data points indicate the initial pool size.

AMPA and NMDA currents

Both types of inputs to MNTB neurons displayed differences between *Diminuendo* wildtype and mutant animals. Both calyceal and non-calyceal EPSCs are mediated by AMPA and NMDA receptor activation (Hamann et al., 2003). Since AMPAR and

NMDAR mediated currents are also involved in development, I studied these currents in more detail in the following experiment.

NMDA and AMPA receptor mediated currents were recorded at holding potentials between -70 and +50 mV incremented in steps of 10 mV. The NMDA current was measured at a time point that corresponds to 5x the fast component of τ_{AMPA} , assuming that the faster AMPA-mediated current is over at this time.

Figure 15A shows two examples both with a large, fast AMPA current. In addition, the neuron on the left displays a slower NMDA current that is absent in the other recording. The NMDA/AMPA ratio calculated for *dmdo/dmdo* mice was with -0.115 ± 0.011 significantly larger than in the control (-0.044 ± 0.004 ; $p < 0.0005$). There was no such difference between Claudin-14 wildtype and mutant mice (-0.034 ± 0.002 and -0.042 ± 0.009 , respectively; $p = 0.37$; Figure 15B). The different NMDA/AMPA ratios in the *Diminuendo* group did not result from differences in the AMPA current amplitudes that were similar (Figure 15C), but from a considerably larger NMDA current in the mutant mice (Figure 15D).

Although the AMPA-mediated currents in the *Diminuendo* group displayed similar amplitudes, bi-exponential fits revealed substantial differences in the decay kinetics. The fast component τ_{fast} was with $293.40 \pm 18.76 \mu\text{s}$ in the mutant significantly slower than in the wildtype (172.78 ± 12.48 ; $p < 0.0005$). Claudin-14 mice showed no such difference (Cldn-14^{+/+}: $220.57 \pm 17.41 \mu\text{s}$, Cldn-14^{-/-}: $230.42 \pm 25.34 \mu\text{s}$, $p = 0.80$; Figure 15E). The slow component τ_{slow} was in *Diminuendo* wildtype mice also faster than in the mutant (DM WT: $1.64 \pm 0.33 \text{ ms}$, *dmdo/dmdo*: $3.01 \pm 0.83 \text{ ms}$; $p = 0.11$). AMPA currents in Claudin-14 mice had a τ_{slow} of $2.19 \pm 0.51 \text{ ms}$ in the control and $1.22 \pm 0.36 \text{ ms}$ in the knockout ($p = 0.14$; Figure 15F).

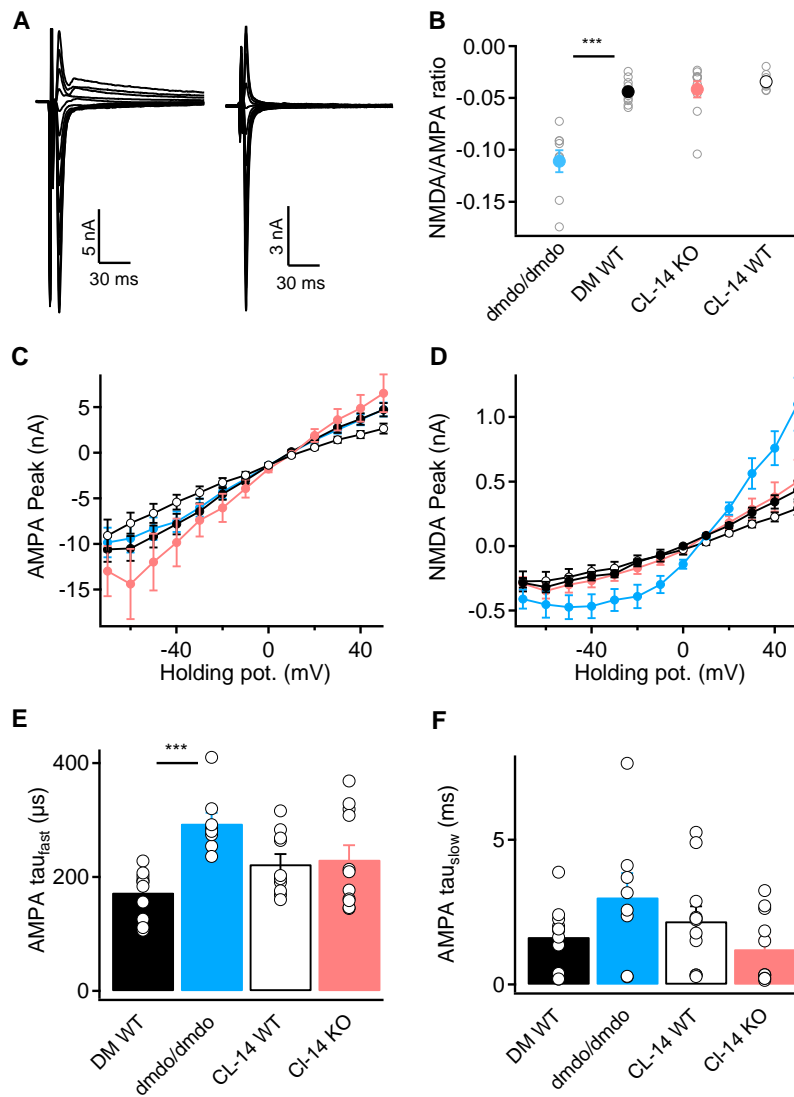


Figure 15: Characterization of AMPA and NMDA currents. **A**: Example recordings of NMDA and AMPA currents evoked at holding potentials between -70 and +50 mV in a cell with (left) and without NMDA currents (right). **B**: Ratio of the NMDA peak to the AMPA peak current. Closed colored symbols represent average values, open circles are individual cells. **C, D**: AMPA (**C**) and NMDA (**D**) currents as a function of the holding potential. **E, F**: The bar graphs show average values for the fast (**E**) and slow (**F**) components of the time constant of the AMPA current. Circles correspond to individual cells. DM WT: n = 11, dmdo/dmdo: n = 8, CL-14 WT: n = 10, CL-14 KO: n = 11.

In summary, this study provides indication for pre- and postsynaptic changes that are specific to the mutation of miR-96 and not a general consequence of hair cell loss. MNTB neurons in homozygous *Diminuendo* mutant mice showed a highly significant decrease in cell diameter and structural deviations at the presynaptic side that were accompanied by changes in the intrinsic properties and alterations in synaptic transmission.

It will be interesting to further analyze the underlying mechanisms that generate the observed differences between *Diminuendo* wildtype and mutant mice. For instance, altered potassium currents could play a role for the changes in firing behavior.

IV. DISCUSSION

The early development and wiring of the auditory system is to a large extent genetically encoded and differs between animals depending on their different demands. The basic tonotopic arrangement is established during fetal and early postnatal life, and thus, without the influence of sensory input, but further activity-dependent refinement occurs during maturation.

In the first set of experiments (Chapter III-1: Development of GABAergic and glycinergic inputs to the LSO in mice and gerbils.), I comparatively studied the developmental changes of the inhibitory MNTB-LSO projection in mice and gerbils before hearing onset. I further analyzed whether the inhibitory neurotransmitters GABA and Glycine are co-released from single vesicles during early postnatal development, a period where this projection undergoes a shift in the predominating transmitter type.

The second study (Chapter II-Characterization of cells and inputs in the adult mouse LSO along the tonotopic axis) examines the LSO of adult mice and addresses the question whether the tonotopic arrangement of this nucleus is reflected in adaptations on the cellular and synaptic level.

In a third series of experiments (Chapter III-3: Consequences of two deafness-related mutations for a large central auditory synapse) I analyzed how the lack of sensory experience affects the calyx of Held and its postsynaptic partners in the MNTB and studied the role of miR-96 for the maturation of this nucleus. Therefore, I compared the Claudin-14 knockout mouse, a mouse model for peripheral hearing loss, to the *Diminuendo* mouse where the mutated miR-96 is expressed in the peripheral and central nervous system.

1. DEVELOPMENT OF GABAERGIC AND GLYCINERGIC INPUTS

The basis for ILD processing in the LSO is a precise balance of the converging excitatory and inhibitory inputs (Boudreau and Tsuchitani, 1968; Sanes, 1990; Grothe et al., 2010). The inhibitory MNTB-LSO projection undergoes major changes before the onset of hearing, including a reduction of inhibitory inputs (Kim and Kandler, 2003) and a decrease in arborization (Sanes and Siverls, 1991).

During early postnatal development, inhibition in this pathway is predominantly GABA-mediated and undergoes a shift to primarily glycinergic transmission that is largely completed around hearing onset (Kotak et al., 1998; Nabekura et al., 2004), a process that contributes to the synaptic refinement of this projection (Kotak and Sanes, 2000; Chang et al., 2003).

In this project, I studied the switch in transmitter type in mice and gerbils at the ages of P 5-6, P 8-9 and P 15-16. Since both species possess differences regarding their hearing range and their required temporal resolution, the question arises whether this is also reflected in differences in the development of the inhibitory MNTB-LSO projection.

Development and species-specific differences

In both mice and gerbils, a developmental increase in the frequency and amplitude of miniature IPSCs was observed, in accordance with literature (Walcher et al.,

2011). An increase in amplitude of miniature postsynaptic currents was also reported for other nuclei of the SOC, such as the MNTB (Taschenberger and von Gersdorff, 2000) and the MSO (Magnusson et al., 2005).

Furthermore, the analysis demonstrated that mIPSCs in both species acquire faster kinetics (Figure 2). An acceleration of the decay time was also observed in the evoked EPSCs while the maximal amplitude remained rather constant in both species (Figure 3). The acquisition of faster IPSC kinetics in both mice and gerbils is in accordance to previously published results in the LSO (Walcher et al., 2011) and was also observed for other nuclei such as the MNTB (Awatramani et al., 2004), the MSO (Magnusson et al., 2005) and the DNLL (Ammer et al., 2012). One factor that could contribute to the acceleration of IPSC kinetics are different GABA and glycine receptor isoforms. The subunit composition changes during development (Piechotta et al., 2001) and influences the IPSC time course (Lynch, 2009).

Contrary to the results reported in Walcher et al. (2011), miniature and evoked IPSCs in the mouse at all studied ages exhibited a generally slower decay time compared to gerbils. Possibly, these slower kinetics in mice are caused by strain-specific differences, as the study mentioned above used Balb/C mice while the results reported here were obtained from C57/BL6 mice. It has been shown previously that different mouse lines exhibit a large variability regarding their auditory function (Zheng, 1999; Myint et al., 2016). One could speculate that the faster IPSC decay kinetics in the Balb/C mouse might lead to a reduced or temporally more precise inhibition in the LSO, but whether this actually leads to changes in ILD processing or is compensated by other intrinsic factors remains to be shown.

No evidence for co-release of GABA and glycine

If there would be a co-release of GABA and glycine from one single synaptic terminal, mIPSCs should exhibit sensitivity to specific blockers. However, in this study, the wash-in of the GABA_A receptor antagonist SR-95531 did not alter the decay time, the amplitude or the frequency significantly (Figure 2).

A co-release of both transmitters from the same vesicles should have resulted in alterations of the mIPSC waveform upon the application of SR-95531. This is in contrast to previously published observations that could demonstrated mixed mIPSCs in the rat (Nabekura et al., 2004) but confirms results obtained in the mouse (Frotscher (2012); unpublished).

A possible explanation could be that mixed mIPSCs occur in the rat but not in mice or gerbils or that the GABAergic component is too small to be detected in these animals. Alternatively, differences in the experimental procedure could have led to these dissimilar results, such as the type of drug used to block GABAergic transmission. While Nabekura et al. (2004) used bicuculline, SR-95531 was applied in this study and in the work of Frotscher (2012). For both drugs, an additional unspecific action on glycine receptors has been demonstrated, that is dependent on the subunit composition and could have influenced the results (Li and Slaughter, 2007).

Furthermore, the wash-in of the blocker did not lead to a reduction of the mIPSC frequency, as it would have been expected for a release of GABA and Glycine from separate vesicles. Assuming that there is actually also GABAergic transmission in the LSO, an explanation for this finding could be a very low release probability of GABA-containing vesicles that is not sufficient to alter the mIPSC frequency significantly.

Indeed, the existence of a GABAergic component could be inferred for evoked IPSCs and was in line with a developmental transition from primarily GABAergic to glycinergic transmission in the mouse LSO (Figure 3). This is in agreement with literature, where the switch in transmitter type has been demonstrated in gerbils and rats by analyzing evoked IPSCs (Kotak et al., 1998; Gillespie et al., 2005).

While the fast component of the decay time was insensitive to SR-95531, the slow component showed a slight reduction in both species. This reduction was more pronounced in the younger age group, suggesting that GABA has a larger contribution in immature animals.

However, these results could not provide evidence for a fast co-release of GABA and glycine in mice and gerbils. The data rather suggest that both transmitters are released separately. The maturation of the inhibitory MNTB-LSO projection in both rodents involves similar developmental changes, such as the acquisition of faster IPSC kinetics. This is not surprising as sound localization with high temporal resolution requires fast and precise signal transmission.

However, this study raises the question where the GABA comes from, as there seems to be no co-release with Glycine from the same vesicle. Furthermore, the results indicate that both inhibitory transmitters could exhibit different release probabilities, arguing against a simultaneous release from the same synaptic terminal. An explanation could be that the GABAergic component demonstrated in the evoked IPSCs is a result of spillover. Indeed, spillover of GABA between neighboring MNTB axons that causes the activation of GABA_A receptors has been recently shown to occur in developing mice (Weisz et al., 2016).

Alternatively, the GABAergic input could originate from an entirely different projection that does not arise in the MNTB. To test this hypothesis, the *Egr2;En1* conditional knockout mouse would be an ideal model, as it does not possess an

MNTB. Studies have shown that mice lacking the MNTB still display a functional glycinergic innervation of the LSO (Jalabi et al., 2013; Altieri et al., 2014), suggesting that inhibition in the LSO may have additional other origins besides the MNTB.

2. CHARACTERIZATION OF CELLS TYPES AND INPUTS IN THE LSO

The LSO receives converging inhibitory and excitatory inputs that are arranged in a frequency-dependent manner and provide the basis for ILD coding (Boudreau and Tsuchitani, 1968, 1970; Moore and Caspary, 1983; Kavanagh and Kelly, 1992). The medial limb preferentially responds to high-frequency sounds while neurons located in the lateral part are more sensitive to sounds with lower frequencies. The following experiments investigate whether the tonotopic gradient in the LSO is accompanied by adaptations in the intrinsic and synaptic properties of neurons sensitive to different frequencies. This study was carried out in the mouse, an animal with a hearing range of relatively high frequencies above 2 kHz (Heffner and Heffner, 2007).

Two different cell types in the LSO

Morphological studies have described between five and seven neuron types in the LSO of rodents and cats (Helfert and Schwartz, 1986, 1987; Rietzel and Friauf, 1998). Electrophysiologically, this study could demonstrate the existence of two different cell populations in the LSO, which display differences regarding their firing behavior, their input resistance and the action potential waveform, but with similar membrane capacitance and resting membrane potential.

The finding of two cell populations is in accordance with Sterenborg et al. (2010), who have also classified two types of neurons in mice: principal neurons that mostly

fire onset action potentials, and continuously spiking lateral olivocochlear (LOC) neurons, that are both evenly distributed within the LSO.

While LSO principal neurons are involved in ILD coding by integrating bilateral converging excitatory and inhibitory inputs, less is known about the function of LOC neurons. They receive input from the ipsilateral PVCN and send efferent projections via the olivocochlear bundle to ipsilateral spiral ganglion neurons that innervate inner hair cells (Felix and Ehrenberger, 1992; Warr, 1992). They are thought to balance interaural sensitivity (Darrow et al., 2006) and play a protective role during noise exposure (Darrow et al., 2007). LOC neurons in the rat (Fujino et al., 1997; Adam et al., 1999) and the mouse (Stereberg et al., 2010) are characterized by distinct properties, including their sustained firing behavior, their higher input resistance compared to principal neurons and distinct current-voltage characteristics.

In this study, the continuously spiking neurons possessed a high input resistance above 500 M Ω and broader action potentials. This cell type was found in the whole LSO except for the most lateral positions and displayed no location-specific adaptations. In contrast, the input resistance of the onset firing neurons was generally lower and increased from medial to lateral. With respect to their higher input resistance and their firing pattern, the continuously firing neurons could therefore indeed be classified as LOC neurons. Furthermore, they were the less prevalent cell type and accounted for approximately one third of all neurons, a ratio that was also previously reported for LOC neurons (Stereberg et al., 2010). However, in contrast to previous findings (Stereberg et al., 2010), these neurons did not differ from principal neurons regarding their membrane capacitance and their resting potential.

Excitatory and inhibitory inputs

LSO neurons are excited by sounds presented to the ipsilateral ear and receive increasing inhibition with increasing sound intensity at the contralateral ear (Boudreau and Tsuchitani, 1968, 1970; Moore and Caspary, 1983; Kavanagh and Kelly, 1992). For ILD coding, the precise timing and strength of the excitatory and inhibitory input is crucial.

The analysis of pharmacologically isolated miniature postsynaptic currents demonstrated larger amplitudes and slower kinetics for inhibitory events compared to excitatory events. Miniature IPSCs occurred with a lower frequency, indicating that LSO neurons receive fewer but stronger inhibitory inputs.

Larger and slower currents were also observed for evoked IPSCs compared to the EPSCs. Especially IPSCs showed discrete amplitude steps with gradually increasing stimulation strength, which is generally interpreted as a recruitment of additional fibers and was also reported in previous studies in mice (Walcher et al., 2011), gerbils (Walcher et al., 2011) and rats (Kim and Kandler, 2003). This stepwise increase in amplitude was less pronounced for EPSCs, suggesting that LSO neurons receive more and smaller excitatory inputs.

Little evidence for tonotopy-dependent adaptations in the mouse LSO

This study found only few hints for cellular and synaptic adaptations to the tonotopic position of the neuron: Onset spiking neurons possibly displayed a gradient regarding their input resistance that increased from the medial to the

lateral LSO while the intrinsic properties of continuously firing cells showed no such relation to their position within the LSO. This would make sense insofar that the onset spiking neurons are presumably principal neurons, and thus, in contrast to the continuously firing LOC neurons, they are involved in ILD coding. Tonotopy-dependent adaptations in the intrinsic properties would therefore rather be expected from these cells than from the LOC neuron. A lower input resistance in the high-frequency medial limb could contribute to a shortening of the integration time, and would therefore improve temporal precision.

On the synaptic side, the characteristics of miniature and evoked IPSCs and EPSCs showed no clear trend from the medial to the lateral limb. If anything, postsynaptic currents in the most laterally located neurons displayed a larger variability.

Taken together, these results indicate that neurons in the mouse LSO hardly possess any considerable adaptations that reflect whether they are involved in the processing of higher or lower frequencies. The lack of any gradients in the properties of LSO neurons contrasts findings from other species with hearing ranges that include lower sound frequencies than the mouse. In the rat and the ferret LSO, a mediolateral gradient was demonstrated for the expression of different proteins such as synaptotagmins (Cooper and Gillespie, 2011), cannabinoid receptors (Chi and Kandler, 2012) and calcium binding proteins (Friauf, 1993; Henkel and Brunso-Bechtold, 1998). A graded expression pattern was also observed for Kv channels that play a role in regulating neuronal excitability (Li et al., 2001; Barnes-Davies et al., 2004).

Presumably, the absence of tonotopy-dependent adaptations in the mouse LSO results from the hearing range of these animals, which is generally quite high and hence, all neurons in the LSO would be already specialized to process these high frequencies and need no further adaptations. It would be interesting to perform the same experiments in an animal with a broader hearing range.

3. CONSEQUENCES OF DEAFNESS-RELATED MUTATIONS

In this study, I compared the consequences of two deafness-related mutations for MNTB principal neurons and their synaptic inputs. *Diminuendo* is the first known mutation of a microRNA associated with deafness and is expressed in the peripheral and central auditory system. While the effects of miR-96 on cochlear development have been investigated before (Lewis et al., 2009; Kuhn et al., 2011), its role in the development of the auditory brainstem was unexplored yet. Since there is no conditional knockout available, the Claudin-14 knockout mouse, where the defect affects only the peripheral auditory system, served as a control.

The MNTB is a suitable nucleus to investigate the consequences of both mutations as it is an early station in auditory processing and acts mainly as a relay rather than fulfilling more complicated integrative functions. The main input to each MNTB principal neuron is provided by one single giant terminal, the calyx of Held, which has become a well-studied model for the analysis of synaptic structure-function relationship. The calyx of Held exhibits little activity-dependent plasticity and develops largely normal in models of congenital hearing loss (Oleskevich et al., 2004; Youssoufian et al., 2005; Youssoufian et al., 2008), an aspect that is helpful to detect alterations induced by the mutation of miR-96 in the brainstem. In contrast, several intrinsic properties of postsynaptic MNTB neurons have been shown to be altered by deafness (Leao et al., 2004; von Hehn et al., 2004; Leao et al., 2006b), making a control with only peripheral deficits necessary.

To reduce possible influences of the tonotopic gradient in neuronal properties (Li et al., 2001; Barnes-Davies et al., 2004; von Hehn et al., 2004; Brew and Forsythe, 2005), all neurons were recorded from the middle part of the MNTB. Despite this limitation, a still impressive heterogeneity was observed in the recordings. This is, however, in agreement with other studies obtained at high temperature, which also showed large variations in their data (Grande et al., 2014).

Comparability of both mutants

The normal development and maturation of sound localization circuits requires genetics, spontaneous activity and sensory experience.

Thus, a suitable control to the *Diminuendo* mouse should exhibit a similar time course and type of developmental defects. Although there is a large number of mouse mutants with hair cell deficiencies available, there is none that mimics the exact cochlear phenotype of the *dmdo/dmdo* mutation, which has been shown to influence the expression of 96 transcripts directly or as a downstream effect, including several genes involved in hair cell function and maturation (Lewis et al., 2009). So far, there is also no conditional knockout of miR-96 in the brainstem available that could serve as control.

In the *dmdo/dmdo* mutant, hair cell development stops at a late embryonic or early postnatal stage. Hair cells fail to differentiate into IHCs and OHCs and retain their immature biophysical properties and morphology before they start to degenerate around P7 (Lewis et al., 2009; Kuhn et al., 2011). In *Cldn-14^{-/-}* mice, the development of the cochlea appears normal during the first postnatal week. This is followed by a

rapid progressive loss of OHCs starting around P 8 and a slower degeneration of IHCs, presumably caused by a failure of the reticular lamina to act as an ionic permeability barrier. Measurements of auditory brainstem responses at P 15 – P 17 demonstrate that *Cldn-14^{-/-}* mice are deaf (Ben-Yosef et al., 2003).

Although the deficiencies in the peripheral system are not identical in these mutants, both the *Cldn-14^{-/-}* and the *dmdo/dmdo* mouse display a similar initial development of the cochlea with a regular morphology and arrangement of hair cells and stereocilia, followed by hair cell loss and deafness. Thus, both mutants should experience normal patterns of spontaneous auditory nerve activity during fetal life, but no refinement dependent on auditory input, making the *Cldn-14^{-/-}* mouse to a sufficient control.

However, mice also exhibit substantial strain-specific differences regarding their auditory function (Zheng, 1999; Myint et al., 2016). Since both mutants are on a different background (NMRI for the *Cldn-14^{-/-}* mouse and C3HeB/FeJ for *Diminuendo*) it is important to compare each mutant to its respective wildtype.

Maturation of synaptic morphology

The calyx of Held features several structural and functional specializations to fulfill its role as fast and largely reliable relay synapse, such as the giant size that allows to harbor large numbers of vesicles and active zones (Satzler et al., 2002). During the first three weeks of life, the cup- or spoon-shaped calyx develops into a complex and highly fenestrated morphology with finger-like substructures and membrane

swellings (Kandler and Friauf, 1993; Satzler et al., 2002; Wimmer et al., 2006; Ford et al., 2009). Within these swellings, the initially more homogeneously distributed vesicles assemble around a cluster of mitochondria, forming a so-called donut around hearing onset (Wimmer et al., 2006). The morphological specializations of the mature calyx of Held are thought to support high-frequency transmission in several ways. For example, the close proximity of vesicles to mitochondria could provide the energy needed for the vesicle cycle. The compartmentalization generated by the membrane swellings could be important to control local calcium and to maintain high concentrations of ATP and glutamate near the active zones (Wimmer et al., 2006).

Immunohistochemical stainings against synaptic vesicle protein 2 (Figure 8) demonstrated well-defined round donuts in the *Diminuendo* wildtype while vesicles in mutant mice were arranged in irregular asymmetric shapes similar to donuts at more immature states shown in Wimmer et al. (2006). In the Claudin-14 group, donuts were generally less uniform and round. A difference between wildtype and mutant was visible but less pronounced, suggesting that deafness may play a role but cannot fully account for the observed differences, indicating that miR-96 is involved in the maturation of the calyx of Held.

Altered synaptic transmission in the Diminuendo mutant

A role of miR-96 in the development of the calyx of Held is further supported by the fact that synapses in mutant mice also exhibit immature features on a functional level, as shown by the analysis of EPSCs.

EPSCs can be described as a product of the number of available vesicles (N), the release probability (P_R) of a single vesicle, and the quantal size q that reflects a single vesicle (Sakaba et al., 2002). Owing to their size, giant synapses such as the calyx of Held can harbor a large number of release sites that determine the maximum N , which can be limited by the rate of pool replenishment. P_R is influenced by intracellular Ca^{2+} and can be increased by elevating the Ca^{2+} concentration, (Borst and Sakmann, 1998; Schneggenburger et al., 1999). Thus, it should be noted that the recording solution used in this study contained a physiological concentration of 1.2 mM Ca^{2+} when comparing these results to other studies of synaptic depression at the calyx of Held.

In all four groups, EPSCs evoked by stimulation of calyceal inputs showed similar peak amplitudes. However, only *dmdo/dmdo* mice demonstrated strong depression compared to the wildtype, especially at higher frequencies (Figure 13). Assuming that depression is to a large degree caused by vesicle pool depletion, cumulative EPSCs were used to estimate the initial pool size (Figure 14). The pool sizes extrapolated from plotting EPSC amplitudes against $EPSC_{cum}$ revealed no differences between normal hearing and deaf mice in the Claudin-14 group. In contrast, pool size estimates for *Diminuendo* mutant mice at 300 and 500 Hz were only 65 and 67 % of the value calculated for the wildtype control. These results further support the view of an arrested development in *dmdo/dmdo* mice since it has been shown that the degree of depression is reduced during development and the estimated vesicle pool increases (Taschenberger and von Gersdorff, 2000; Taschenberger et al., 2002).

These results also confirm the close relationship of structure and function at the calyx of Held. The mature morphology with its donut-like arrangement of vesicles (Figure 8) is thought to support high frequency transmission for longer periods of

time (Wimmer et al., 2006). The *Diminuendo* control mouse with the most defined donuts shows less depression and a larger pool size estimate than the other groups. However, the differences especially at high-frequency stimulations are not necessarily caused only by presynaptic differences but could be partly also generated postsynaptically by AMPA receptor saturation and desensitization (Neher and Sakaba, 2001; Scheuss et al., 2002).

In all groups, MNTB neurons received smaller non-calyceal inputs in addition to the large calyceal input (Figure 13). These inputs were also mentioned in previous studies (Forsythe and Barnes-Davies, 1993; Smith et al., 1998; Taschenberger and von Gersdorff, 2000; Hamann et al., 2003) but their function and origin remains largely unclear. Due to their differences in threshold and kinetics, it is assumed that they do not originate from globular bushy cells. Possibly, they arise from SBCs in the contralateral AVCN and have a modulatory effect on the calyceal input (Hamann et al., 2003).

These inputs were clearly different from the calyceal inputs and are characterized by a smaller amplitude and slower kinetics, consistent with literature (Hamann et al., 2003). Furthermore, they often displayed facilitation upon train stimulation at lower frequencies that was more pronounced in the normal hearing animals, suggesting that activity-dependent mechanisms may play a role in the development of the non-calyceal inputs.

Immature AMPAR and NMDAR mediated currents in Diminuendo mice

The study of NMDA and AMPA receptor mediated currents revealed differences between the *dmdo/dmdo* mouse and the other groups (Figure 15). Both AMPA and NMDA receptors are activated by glutamate. Their different kinetics lead to a biphasic response with a slower NMDA component and a faster AMPA component. Several studies demonstrate that the initially large amplitude of NMDAR mediated currents in pre-hearing animals is strongly reduced during maturation, a process that is thought to contribute to fast high-fidelity synaptic transmission (Taschenberger and von Gersdorff, 2000; Futai et al., 2001; Joshi and Wang, 2002; Steinert et al., 2010).

Interestingly, substantial NMDAR current amplitudes were only observed in *dmdo/dmdo* mice but not in the other groups while AMPAR current amplitudes did not differ from the wildtype, leading to a significantly altered NMDA/AMPA ratio in the *Diminuendo* mutant (Figure 15 B - D). This prominent difference was also confirmed by blind analysis – *Diminuendo* mutant and wildtype mice were correctly identified in about 80 % of the cells, while Claudin.14 knockout and wildtype mice were undistinguishable. Deafness had no influence on the NMDA/AMPA ratio as also indicated by the similar values in the Claudin14 group, suggesting that miR-96 takes part in the development of mature NMDAR current characteristics in MNTB principal neurons.

In addition, AMPAR mediated currents demonstrated significantly slower kinetics in the *Diminuendo* mutant (Figure 15 E, F). It has been shown that AMPAR currents acquire faster kinetics during development (Taschenberger and von Gersdorff, 2000; Koike-Tani et al., 2005), further supporting the assumption that the miR-96 mutation disrupts the maturation of glutamatergic transmission in the MNTB.

Alteration of specific intrinsic properties by the miR-96 mutation

In contrast to many aspects of synaptic morphology and transmission that were clearly influenced by miR-96, several passive properties and action potential parameters of MNTB principal neurons remained to a large extent unchanged by the *Diminuendo* mutation and by deafness in general.

Although the average cell diameter estimated from immunostainings was significantly reduced by about 11 % in the *Diminuendo* mutant (Figure 8), this difference in size was not significant in effective membrane capacitance measurements (Figure 9). Both deaf mice exhibited a slightly lower, but not significantly altered input resistance and showed no clear differences regarding their membrane time constants. This is consistent with previous studies that demonstrated that hearing loss has no considerable effect on these passive parameters (Leao et al., 2005; Leao et al., 2006a; Grimsley and Sivaramakrishnan, 2014). These results also indicate that the mutation of miR-96 has only little consequences for the development of the approximated passive cell properties.

The analysis of several action potential parameters revealed that neither deafness in general nor the mutation of miR-96 altered the shape and thresholds considerably (Figure 11). Only the current threshold in cells of *Diminuendo* mutant mice showed a nearly significant reduction. It has been shown that action potentials in MNTB principal neurons acquire higher current thresholds during development (Hoffpauir et al., 2010).

Thus, this could be an additional hint for the theory of a developmental arrest. Alternatively, the reduced current threshold could reflect a generally elevated excitability as previously described for deaf mice (Leao et al., 2004)

Although these results demonstrated no clear effects of any of the mutations, they emphasize the large strain-specific differences between the NMRI and C3HeB/FeJ mice.

Despite the largely unchanged action potential parameters elicited by short EPSC-approximating stimuli, long depolarizations demonstrated clear differences in excitability. In the *Diminuendo* mouse, a larger proportion of cells exhibited a tonic firing behavior compared to the wildtype (Figure 10), again indicating that certain neuronal properties remain developmentally premature. Studies demonstrate that a continuous firing behavior is characteristic for young animals while an onset-firing type predominates in MNTB neurons of mature animals (Dodson et al., 2002; Hoffpauir et al., 2010). Pharmacological evidence, immunohistochemistry and gene expression studies have revealed that low-voltage activated potassium channels play a major role in controlling the firing behavior and that the expression of different subtypes is developmentally regulated (Brew and Forsythe, 1995; Leao et al., 2004; Hoffpauir et al., 2010).

It will be interesting to address the question whether the observed changes in firing behavior of MNTB neurons in the *Diminuendo* mouse are a consequence of an immature expression pattern of these channels. This could be realized by different approaches, such as pharmacological or Immunohistochemical methods or by analyzing expression levels of calcium channel mRNA.

The fact that both firing types occur with the same frequency in normal hearing and deaf mice of the Claudin-14 group indicates that hair cell defects alone are not sufficient to alter the firing behavior. Conversely, MNTB neurons in the *deafness* (dn/dn) mouse, another commonly used model for deafness caused by cochlear defects, have been shown to exhibit a predominance of the sustained firing pattern comparable to the *Diminuendo* mouse (Oleskevich and Walmsley, 2002). In this

mutant, the degeneration of the organ of Corti starts around P15, but some structural abnormalities are already present at birth (Faddis et al., 1998).

Summary and outlook

The comparison of the *Diminuendo* mutant and the Claudin-14 knockout mouse revealed several features of the calyx of Held. First, it is notable that the maturation of the calyx of Held and its postsynaptic partner show little activity-dependent plasticity and seem to follow a developmental program that is barely influenced by hair cell degeneration, as indicated by the results obtained from the Claudin-14 knockout mice. The majority of the results showed no differences between hearing-impaired and control animals: the passive and active intrinsic membrane properties of MNTB principal neurons were not distinguishable and both groups exhibited similar firing patterns and action potential characteristics, as well as equal levels of depression of calyceal EPSCs, a similar vesicle pool estimate and a comparable NMDA/AMPA ratio.

In the *Diminuendo* group, the differences between mutant and wildtype mice were more pronounced. These alterations appear to reflect a developmentally premature state of the calyx of Held and some features of the postsynaptic neuron rather than a compensation for the lack of normal auditory experience. The presynaptic terminal displays an immature morphology that is accompanied by several features of synaptic transmission characteristic for younger animals, such as a stronger depression of EPSCs and immature proportions and kinetics of NMDA and AMPA receptor mediated currents. In addition, neurons are more excitable and

only a minority responds with an adult-like firing pattern. The fact that some parameters are not altered by the mutation indicates that it does not lead to a general developmental arrest but that is involved in the maturation of certain specific neuronal and synaptic properties.

Furthermore, this work shows that mice exhibit considerable strain-specific differences that should not be underestimated when comparing results from different mouse lines. But even if the mice investigated here would have had the same background, the comparison of these two mutations has limitations as both affect cochlear development in their own complex ways, which could have downstream consequences that are hard to predict. Thus, the next step would be to create a conditional knockout of miR-96 in the auditory brainstem.

Despite these limitations, the findings reported in this study provide evidence that miR-96 is not only involved in the development of the cochlea but that it also regulates the maturation of auditory brainstem nuclei. These results may also contribute to the understanding of miR-96 mutations related to hearing loss in humans. For instance, to predict the outcome of a treatment with a cochlea implant, it is important to know whether the central auditory pathway is actually functional.

LITERATURE

- Adam TJ, Schwarz DW, Finlayson PG (1999) Firing properties of chopper and delay neurons in the lateral superior olive of the rat. *Experimental brain research* 124:489-502.
- Adams J (1997) Projections from octopus cells of the posteroventral cochlear nucleus to the ventral nucleus of the lateral lemniscus in cat and human. *Auditory Neuroscience* 3:335-350.
- Altieri SC, Zhao T, Jalabi W, Maricich SM (2014) Development of glycinergic innervation to the murine LSO and SPN in the presence and absence of the MNTB. *Frontiers in neural circuits* 8:109.
- Ammer JJ, Grothe B, Felmy F (2012) Late postnatal development of intrinsic and synaptic properties promotes fast and precise signaling in the dorsal nucleus of the lateral lemniscus. *Journal of neurophysiology* 107:1172-1185.
- Awatramani GB, Turecek R, Trussell LO (2004) Inhibitory control at a synaptic relay. *The Journal of neuroscience : the official journal of the Society for Neuroscience* 24:2643-2647.
- Barnes-Davies M, Barker MC, Osmani F, Forsythe ID (2004) Kv1 currents mediate a gradient of principal neuron excitability across the tonotopic axis in the rat lateral superior olive. *The European journal of neuroscience* 19:325-333.
- Bear MF, Connors BW, Paradiso MA (2007) *Neuroscience: Exploring the brain*: Lippincott Williams & Wilkins.
- Ben-Yosef T, Belyantseva IA, Saunders TL, Hughes ED, Kawamoto K, Van Itallie CM, Beyer LA, Halsey K, Gardner DJ, Wilcox ER, Rasmussen J, Anderson JM, Dolan DF, Forge A, Raphael Y, Camper SA, Friedman TB (2003) Claudin 14 knockout mice, a model for autosomal recessive deafness DFNB29, are deaf due to cochlear hair cell degeneration. *Human molecular genetics* 12:2049-2061.
- Berger C, Meyer EM, Ammer JJ, Felmy F (2014) Large somatic synapses on neurons in the ventral lateral lemniscus work in pairs. *The Journal of neuroscience : the official journal of the Society for Neuroscience* 34:3237-3246.
- Borst JG, Sakmann B (1998) Calcium current during a single action potential in a large presynaptic terminal of the rat brainstem. *The Journal of physiology* 506 (Pt 1):143-157.
- Borst JG, Soria van Hoeve J (2012) The calyx of Held synapse: from model synapse to auditory relay. *Annual review of physiology* 74:199-224.
- Bortone DS, Mitchell K, Manis PB (2006) Developmental time course of potassium channel expression in the rat cochlear nucleus. *Hearing research* 211:114-125.
- Boudreau JC, Tsuchitani C (1968) Binaural interaction in the cat superior olive S segment. *Journal of neurophysiology* 31:442-454.
- Boudreau JC, Tsuchitani C (1970) Cat superior olive S-segment cell discharge to tonal stimulation. *Contributions to sensory physiology* 4:143-213.

- Brew HM, Forsythe ID (1995) Two voltage-dependent K⁺ conductances with complementary functions in postsynaptic integration at a central auditory synapse. *The Journal of neuroscience : the official journal of the Society for Neuroscience* 15:8011-8022.
- Brew HM, Forsythe ID (2005) Systematic variation of potassium current amplitudes across the tonotopic axis of the rat medial nucleus of the trapezoid body. *Hearing research* 206:116-132.
- Brown SD, Hardisty-Hughes RE, Mburu P (2008) Quiet as a mouse: dissecting the molecular and genetic basis of hearing. *Nature reviews Genetics* 9:277-290.
- Brown SDM, Peters J (1996) Combining mutagenesis and genomics in the mouse — closing the phenotype gap. *Trends in Genetics* 12:433-435.
- Cant NB, Benson CG (2003) Parallel auditory pathways: projection patterns of the different neuronal populations in the dorsal and ventral cochlear nuclei. *Brain Research Bulletin* 60:457-474.
- Chang EH, Kotak VC, Sanes DH (2003) Long-term depression of synaptic inhibition is expressed postsynaptically in the developing auditory system. *Journal of neurophysiology* 90:1479-1488.
- Charif M, Boulouiz R, Bakhechane A, Benrahma H, Nahili H, Eloualid A, Rouba H, Kandil M, Abidi O, Lenaers G, Barakat A (2013) Genetic and molecular analysis of the CLDN14 gene in Moroccan family with non-syndromic hearing loss. *Indian journal of human genetics* 19:331-336.
- Chi DH, Kandler K (2012) Cannabinoid receptor expression at the MNTB-LSO synapse in developing rats. *Neuroscience letters* 509:96-100.
- Cooper AP, Gillespie DC (2011) Synaptotagmins I and II in the developing rat auditory brainstem: Synaptotagmin I is transiently expressed in glutamate-releasing immature inhibitory terminals. *The Journal of comparative neurology* 519:2417-2433.
- Covey E, Casseday JH (1986) Connectional basis for frequency representation in the nuclei of the lateral lemniscus of the bat *Eptesicus fuscus*. *The Journal of neuroscience : the official journal of the Society for Neuroscience* 6:2926-2940.
- Covey E, Casseday JH (1991) The monaural nuclei of the lateral lemniscus in an echolocating bat: parallel pathways for analyzing temporal features of sound. *The Journal of neuroscience : the official journal of the Society for Neuroscience* 11:3456-3470.
- Cramer KS, Gabriele ML (2014) Axon guidance in the auditory system: multiple functions of Eph receptors. *Neuroscience* 277:152-162.
- Darrow KN, Maison SF, Liberman MC (2006) Cochlear efferent feedback balances interaural sensitivity. *Nature neuroscience* 9:1474-1476.
- Darrow KN, Maison SF, Liberman MC (2007) Selective removal of lateral olivocochlear efferents increases vulnerability to acute acoustic injury. *Journal of neurophysiology* 97:1775-1785.
- Davis GM, Haas MA, Pockock R (2015) MicroRNAs: Not “Fine-Tuners” but Key Regulators of Neuronal Development and Function. *Frontiers in Neurology* 6:245.
- del Castillo I, Villamar M, Moreno-Pelayo MA, del Castillo FJ, Alvarez A, Telleria D, Menendez I, Moreno F (2002) A deletion involving the connexin 30 gene in nonsyndromic hearing impairment. *The New England journal of medicine* 346:243-249.
- Di Bonito M, Narita Y, Avallone B, Sequino L, Mancuso M, Andolfi G, Franze AM, Puellas L, Rijli FM, Studer M (2013) Assembly of the auditory circuitry by a Hox genetic network in the mouse brainstem. *PLoS genetics* 9:e1003249.

- Dodson PD, Barker MC, Forsythe ID (2002) Two heteromeric Kv1 potassium channels differentially regulate action potential firing. *The Journal of neuroscience : the official journal of the Society for Neuroscience* 22:6953-6961.
- Dror AA, Avraham KB (2010) Hearing impairment: a panoply of genes and functions. *Neuron* 68:293-308.
- Elmqvist D, Quastel DM (1965) A quantitative study of end-plate potentials in isolated human muscle. *The Journal of physiology* 178:505-529.
- Faddis BT, Hughes RM, Miller JD (1998) Quantitative measures reflect degeneration, but not regeneration, in the deafness mouse organ of Corti. *Hearing research* 115:6-12.
- Felix D, Ehrenberger K (1992) The efferent modulation of mammalian inner hair cell afferents. *Hearing research* 64:1-5.
- Ford MC, Grothe B, Klug A (2009) Fenestration of the calyx of Held occurs sequentially along the tonotopic axis, is influenced by afferent activity, and facilitates glutamate clearance. *The Journal of comparative neurology* 514:92-106.
- Forsythe ID, Barnes-Davies M (1993) The binaural auditory pathway: excitatory amino acid receptors mediate dual timecourse excitatory postsynaptic currents in the rat medial nucleus of the trapezoid body. *Proceedings Biological sciences / The Royal Society* 251:151-157.
- Franzen DL, Gleiss SA, Berger C, Kumpfbeck FS, Ammer JJ, Felmy F (2015) Development and modulation of intrinsic membrane properties control the temporal precision of auditory brain stem neurons. *Journal of neurophysiology* 113:524-536.
- Friauf E (1993) Transient appearance of calbindin-D28k-positive neurons in the superior olivary complex of developing rats. *The Journal of comparative neurology* 334:59-74.
- Friauf E, Ostwald J (1988) Divergent projections of physiologically characterized rat ventral cochlear nucleus neurons as shown by intra-axonal injection of horseradish peroxidase. *Experimental brain research* 73:263-284.
- Friauf E, Lohmann C (1999) Development of auditory brainstem circuitry. Activity-dependent and activity-independent processes. *Cell and tissue research* 297:187-195.
- Friedman RC, Farh KK, Burge CB, Bartel DP (2009) Most mammalian mRNAs are conserved targets of microRNAs. *Genome research* 19:92-105.
- Frotscher E (2012) Analyse pharmakologisch isolierter „miniature events“ an LSO Neuronen in Wildtyp und CaV1.3 knock-out Mäusen. In: bachelor thesis, TU Kaiserslautern.
- Fujino K, Koyano K, Ohmori H (1997) Lateral and medial olivocochlear neurons have distinct electrophysiological properties in the rat brain slice. *Journal of neurophysiology* 77:2788-2804.
- Futai K, Okada M, Matsuyama K, Takahashi T (2001) High-fidelity transmission acquired via a developmental decrease in NMDA receptor expression at an auditory synapse. *The Journal of neuroscience : the official journal of the Society for Neuroscience* 21:3342-3349.
- Gibson F, Walsh J, Mburu P, Varela A, Brown KA, Antonio M, Beisel KW, Steel KP, Brown SD (1995) A type VII myosin encoded by the mouse deafness gene shaker-1. *Nature* 374:62-64.
- Gillespie DC, Kim G, Kandler K (2005) Inhibitory synapses in the developing auditory system are glutamatergic. *Nature neuroscience* 8:332-338.
- Grande G, Negandhi J, Harrison RV, Wang LY (2014) Remodelling at the calyx of Held-MNTB synapse in mice developing with unilateral conductive hearing loss. *The Journal of physiology* 592:1581-1600.

- Gratton MA, Vazquez AE (2003) Age-related hearing loss: current research. *Current opinion in otolaryngology & head and neck surgery* 11:367-371.
- Grimsley CA, Sivaramakrishnan S (2014) Postnatal developmental changes in the medial nucleus of the trapezoid body in a mouse model of auditory pathology. *Neuroscience letters* 559:152-157.
- Grimson A, Srivastava M, Fahey B, Woodcroft BJ, Chiang HR, King N, Degnan BM, Rokhsar DS, Bartel DP (2008) Early origins and evolution of microRNAs and Piwi-interacting RNAs in animals. *Nature* 455:1193-1197.
- Grothe B (2000) The evolution of temporal processing in the medial superior olive, an auditory brainstem structure. *Progress in neurobiology* 61:581-610.
- Grothe B (2003) New roles for synaptic inhibition in sound localization. *Nature reviews Neuroscience* 4:540-550.
- Grothe B, Pecka M, McAlpine D (2010) Mechanisms of sound localization in mammals. *Physiological reviews* 90:983-1012.
- Hamann M, Billups B, Forsythe ID (2003) Non-calyceal excitatory inputs mediate low fidelity synaptic transmission in rat auditory brainstem slices. *The European journal of neuroscience* 18:2899-2902.
- Heffner HE, Heffner RS (2007) Hearing ranges of laboratory animals. *Journal of the American Association for Laboratory Animal Science : JAALAS* 46:20-22.
- Helfert RH, Schwartz IR (1986) Morphological evidence for the existence of multiple neuronal classes in the cat lateral superior olivary nucleus. *The Journal of comparative neurology* 244:533-549.
- Helfert RH, Schwartz IR (1987) Morphological features of five neuronal classes in the gerbil lateral superior olive. *The American journal of anatomy* 179:55-69.
- Henkel CK, Brunso-Bechtold JK (1998) Calcium-binding proteins and GABA reveal spatial segregation of cell types within the developing lateral superior olivary nucleus of the ferret. *Microscopy Research and Technique* 41:234-245.
- Hoffpauir BK, Grimes JL, Mathers PH, Spirou GA (2006) Synaptogenesis of the calyx of Held: rapid onset of function and one-to-one morphological innervation. *The Journal of neuroscience : the official journal of the Society for Neuroscience* 26:5511-5523.
- Hoffpauir BK, Kolson DR, Mathers PH, Spirou GA (2010) Maturation of synaptic partners: functional phenotype and synaptic organization tuned in synchrony. *The Journal of physiology* 588:4365-4385.
- Hou J (2012) The yin and yang of claudin-14 function in human diseases. *Annals of the New York Academy of Sciences* 1258:185-190.
- Iwasaki S, Takahashi T (1998) Developmental changes in calcium channel types mediating synaptic transmission in rat auditory brainstem. *The Journal of physiology* 509:419-423.
- Jalabi W, Kopp-Scheinpflug C, Allen PD, Schiavon E, DiGiacomo RR, Forsythe ID, Maricich SM (2013) Sound Localization Ability and Glycinergic Innervation of the Superior Olivary Complex Persist after Genetic Deletion of the Medial Nucleus of the Trapezoid Body. *The Journal of Neuroscience* 33:15044-15049.
- Joshi I, Wang LY (2002) Developmental profiles of glutamate receptors and synaptic transmission at a single synapse in the mouse auditory brainstem. *The Journal of physiology* 540:861-873.
- Kakazu Y, Akaike N, Komiyama S, Nabekura J (1999) Regulation of intracellular chloride by cotransporters in developing lateral superior olive neurons. *The Journal of neuroscience : the official journal of the Society for Neuroscience* 19:2843-2851.

- Kandler K, Friauf E (1993) Pre- and postnatal development of efferent connections of the cochlear nucleus in the rat. *The Journal of comparative neurology* 328:161-184.
- Kandler K, Friauf E (1995) Development of glycinergic and glutamatergic synaptic transmission in the auditory brainstem of perinatal rats. *The Journal of neuroscience : the official journal of the Society for Neuroscience* 15:6890-6904.
- Kandler K, Clause A, Noh J (2009) Tonotopic reorganization of developing auditory brainstem circuits. *Nature neuroscience* 12:711-717.
- Kapfer C, Seidl AH, Schweizer H, Grothe B (2002) Experience-dependent refinement of inhibitory inputs to auditory coincidence-detector neurons. *Nature neuroscience* 5:247-253.
- Kavanagh GL, Kelly JB (1992) Midline and lateral field sound localization in the ferret (*Mustela putorius*): contribution of the superior olivary complex. *Journal of neurophysiology* 67:1643-1658.
- Kelsell DP, Dunlop J, Stevens HP, Lench NJ, Liang JN, Parry G, Mueller RF, Leigh IM (1997) Connexin 26 mutations in hereditary non-syndromic sensorineural deafness. *Nature* 387:80-83.
- Kil J, Kageyama GH, Semple MN, Kitzes LM (1995) Development of ventral cochlear nucleus projections to the superior olivary complex in gerbil. *The Journal of comparative neurology* 353:317-340.
- Kim G, Kandler K (2003) Elimination and strengthening of glycinergic/GABAergic connections during tonotopic map formation. *Nature neuroscience* 6:282-290.
- Kitzes LM, Kageyama GH, Semple MN, Kil J (1995) Development of ectopic projections from the ventral cochlear nucleus to the superior olivary complex induced by neonatal ablation of the contralateral cochlea. *The Journal of comparative neurology* 353:341-363.
- Kloosterman WP, Plasterk RHA (2006) The Diverse Functions of MicroRNAs in Animal Development and Disease. *Developmental Cell* 11:441-450.
- Koike-Tani M, Saitoh N, Takahashi T (2005) Mechanisms underlying developmental speeding in AMPA-EPSC decay time at the calyx of Held. *The Journal of neuroscience : the official journal of the Society for Neuroscience* 25:199-207.
- Korada S, Schwartz IR (1999) Development of GABA, glycine, and their receptors in the auditory brainstem of gerbil: a light and electron microscopic study. *The Journal of comparative neurology* 409:664-681.
- Kotak VC, Sanes DH (2000) Long-lasting inhibitory synaptic depression is age- and calcium-dependent. *The Journal of neuroscience : the official journal of the Society for Neuroscience* 20:5820-5826.
- Kotak VC, Korada S, Schwartz IR, Sanes DH (1998) A developmental shift from GABAergic to glycinergic transmission in the central auditory system. *The Journal of neuroscience : the official journal of the Society for Neuroscience* 18:4646-4655.
- Koundakjian EJ, Appler JL, Goodrich LV (2007) Auditory neurons make stereotyped wiring decisions before maturation of their targets. *The Journal of neuroscience : the official journal of the Society for Neuroscience* 27:14078-14088.
- Kremer H, van Wijk E, Marker T, Wolfrum U, Roepman R (2006) Usher syndrome: molecular links of pathogenesis, proteins and pathways. *Human molecular genetics* 15 Spec No 2:R262-270.
- Kuhn S, Johnson SL, Furness DN, Chen J, Ingham N, Hilton JM, Steffes G, Lewis MA, Zampini V, Hackney CM, Masetto S, Holley MC, Steel KP, Marcotti W (2011) miR-96 regulates the progression of differentiation in mammalian cochlear inner and outer hair cells.

- Proceedings of the National Academy of Sciences of the United States of America 108:2355-2360.
- Kullmann PH, Kandler K (2001) Glycinergic/GABAergic synapses in the lateral superior olive are excitatory in neonatal C57Bl/6J mice. *Brain research Developmental brain research* 131:143-147.
- Kullmann PH, Ene FA, Kandler K (2002) Glycinergic and GABAergic calcium responses in the developing lateral superior olive. *The European journal of neuroscience* 15:1093-1104.
- Leao RN, Berntson A, Forsythe ID, Walmsley B (2004) Reduced low-voltage activated K⁺ conductances and enhanced central excitability in a congenitally deaf (dn/dn) mouse. *The Journal of physiology* 559:25-33.
- Leao RN, Svahn K, Berntson A, Walmsley B (2005) Hyperpolarization-activated (I_h) currents in auditory brainstem neurons of normal and congenitally deaf mice. *European Journal of Neuroscience* 22:147-157.
- Leao RN, Naves MM, Leão KE, Walmsley B (2006a) Altered sodium currents in auditory neurons of congenitally deaf mice. *European Journal of Neuroscience* 24:1137-1146.
- Leao RN, Sun H, Svahn K, Berntson A, Youssoufian M, Paolini AG, Fyffe RE, Walmsley B (2006b) Topographic organization in the auditory brainstem of juvenile mice is disrupted in congenital deafness. *The Journal of physiology* 571:563-578.
- Lee K, Ansar M, Andrade PB, Khan B, Santos-Cortez RL, Ahmad W, Leal SM (2012) Novel CLDN14 mutations in Pakistani families with autosomal recessive non-syndromic hearing loss. *American journal of medical genetics Part A* 158a:315-321.
- Lewis MA, Quint E, Glazier AM, Fuchs H, De Angelis MH, Langford C, van Dongen S, Abreu-Goodger C, Piipari M, Redshaw N, Dalmay T, Moreno-Pelayo MA, Enright AJ, Steel KP (2009) An ENU-induced mutation of miR-96 associated with progressive hearing loss in mice. *Nature genetics* 41:614-618.
- Li P, Slaughter M (2007) Glycine receptor subunit composition alters the action of GABA antagonists. *Visual neuroscience* 24:513-521.
- Li W, Kaczmarek LK, Perney TM (2001) Localization of two high-threshold potassium channel subunits in the rat central auditory system. *The Journal of comparative neurology* 437:196-218.
- Lynch JW (2009) Native glycine receptor subtypes and their physiological roles. *Neuropharmacology* 56:303-309.
- Madara JL (1998) Regulation of the movement of solutes across tight junctions. *Annual review of physiology* 60:143-159.
- Magnusson AK, Kapfer C, Grothe B, Koch U (2005) Maturation of glycinergic inhibition in the gerbil medial superior olive after hearing onset. *The Journal of physiology* 568:497-512.
- Mathur P, Yang J (2015) Usher syndrome: Hearing loss, retinal degeneration and associated abnormalities. *Biochimica et biophysica acta* 1852:406-420.
- Mburu P et al. (2003) Defects in whirlin, a PDZ domain molecule involved in stereocilia elongation, cause deafness in the whirler mouse and families with DFNB31. *Nature genetics* 34:421-428.
- McAlpine D, Grothe B (2003) Sound localization and delay lines--do mammals fit the model? *Trends in neurosciences* 26:347-350.
- Mencia A, Modamio-Hoybjor S, Redshaw N, Morin M, Mayo-Merino F, Olavarrieta L, Aguirre LA, del Castillo I, Steel KP, Dalmay T, Moreno F, Moreno-Pelayo MA (2009) Mutations in the seed region of human miR-96 are responsible for nonsyndromic progressive hearing loss. *Nature genetics* 41:609-613.

- Michalski N, Babai N, Renier N, Perkel DJ, Chedotal A, Schneggenburger R (2013) Robo3-driven axon midline crossing conditions functional maturation of a large commissural synapse. *Neuron* 78:855-868.
- Moore MJ, Caspary DM (1983) Strychnine blocks binaural inhibition in lateral superior olivary neurons. *The Journal of neuroscience : the official journal of the Society for Neuroscience* 3:237-242.
- Myint A, White CH, Ohmen JD, Li X, Wang J, Lavinsky J, Salehi P, Crow AL, Ohyama T, Friedman RA (2016) Large-scale phenotyping of noise-induced hearing loss in 100 strains of mice. *Hearing research* 332:113-120.
- Nabekura J, Katsurabayashi S, Kakazu Y, Shibata S, Matsubara A, Jinno S, Mizoguchi Y, Sasaki A, Ishibashi H (2004) Developmental switch from GABA to glycine release in single central synaptic terminals. *Nature neuroscience* 7:17-23.
- Nakamura PA, Cramer KS (2011) Formation and maturation of the calyx of Held. *Hearing research* 276:70-78.
- Neher E, Sakaba T (2001) Combining deconvolution and noise analysis for the estimation of transmitter release rates at the calyx of held. *The Journal of neuroscience : the official journal of the Society for Neuroscience* 21:444-461.
- Nickel R, Forge A (2008) Gap junctions and connexins in the inner ear: their roles in homeostasis and deafness. *Current opinion in otolaryngology & head and neck surgery* 16:452-457.
- Nishio SY, Hattori M, Moteki H, Tsukada K, Miyagawa M, Naito T, Yoshimura H, Iwasa Y, Mori K, Shima Y, Sakuma N, Usami S (2015) Gene expression profiles of the cochlea and vestibular endorgans: localization and function of genes causing deafness. *The Annals of otology, rhinology, and laryngology* 124 Suppl 1:6s-48s.
- Nolan PM et al. (2000) A systematic, genome-wide, phenotype-driven mutagenesis programme for gene function studies in the mouse. *Nature genetics* 25:440-443.
- Oleskevich S, Walmsley B (2002) Synaptic transmission in the auditory brainstem of normal and congenitally deaf mice. *The Journal of physiology* 540:447-455.
- Oleskevich S, Youssoufian M, Walmsley B (2004) Presynaptic plasticity at two giant auditory synapses in normal and deaf mice. *The Journal of physiology* 560:709-719.
- Palma FD, Holme RH, Bryda EC, Belyantseva IA, Pellegrino R, Kachar B, Steel KP, Noben-Trauth K (2001) Mutations in *Cdh23*, encoding a new type of cadherin, cause stereocilia disorganization in waltzer, the mouse model for Usher syndrome type 1D. *Nature genetics* 27:103-107.
- Piechotta K, Weth F, Harvey RJ, Friauf E (2001) Localization of rat glycine receptor $\alpha 1$ and $\alpha 2$ subunit transcripts in the developing auditory brainstem. *The Journal of comparative neurology* 438:336-352.
- Pollak GD, Gittelman JX, Li N, Xie R (2011) Inhibitory projections from the ventral nucleus of the lateral lemniscus and superior paraolivary nucleus create directional selectivity of frequency modulations in the inferior colliculus: a comparison of bats with other mammals. *Hearing research* 273:134-144.
- Rautenberg PL, Grothe B, Felmy F (2009) Quantification of the three-dimensional morphology of coincidence detector neurons in the medial superior olive of gerbils during late postnatal development. *The Journal of comparative neurology* 517:385-396.
- Raviv D, Dror AA, Avraham KB (2010) Hearing loss: a common disorder caused by many rare alleles. *Annals of the New York Academy of Sciences* 1214:168-179.

- Rhode W, Oertel D, Smith P (1983) Physiological response properties of cells labeled intracellularly with horseradish peroxidase in cat ventral cochlear nucleus. *Journal of Comparative Neurology* 213:448-463.
- Richardson GP, de Monvel JB, Petit C (2011) How the genetics of deafness illuminates auditory physiology. *Annual review of physiology* 73:311-334.
- Rietzel HJ, Friauf E (1998) Neuron types in the rat lateral superior olive and developmental changes in the complexity of their dendritic arbors. *The Journal of comparative neurology* 390:20-40.
- Rosengauer E, Hartwich H, Hartmann AM, Rudnicki A, Satheesh SV, Avraham KB, Nothwang HG (2012) *Egr2::cre* mediated conditional ablation of *dicer* disrupts histogenesis of mammalian central auditory nuclei. *PLoS one* 7:e49503.
- Roux I, Safieddine S, Nouvian R, Grati M, Simmler MC, Bahloul A, Perfettini I, Le Gall M, Rostaing P, Hamard G, Triller A, Avan P, Moser T, Petit C (2006) Otoferlin, defective in a human deafness form, is essential for exocytosis at the auditory ribbon synapse. *Cell* 127:277-289.
- Ruel J, Emery S, Nouvian R, Bersot T, Amilhon B, Van Rybroek JM, Rebillard G, Lenoir M, Eybalin M, Delprat B, Sivakumaran TA, Giros B, El Mestikawy S, Moser T, Smith RJ, Lesperance MM, Puel JL (2008) Impairment of SLC17A8 encoding vesicular glutamate transporter-3, VGLUT3, underlies nonsyndromic deafness DFNA25 and inner hair cell dysfunction in null mice. *American journal of human genetics* 83:278-292.
- Ruepp A, Kowarsch A, Schmidl D, Buggenthin F, Brauner B, Dunger I, Fobo G, Frishman G, Montrone C, Theis FJ (2010) PhenomiR: a knowledgebase for microRNA expression in diseases and biological processes. *Genome biology* 11:R6.
- Rusu SI, Borst JG (2011) Developmental changes in intrinsic excitability of principal neurons in the rat medial nucleus of the trapezoid body. *Dev Neurobiol* 71:284-295.
- Sakaba T, Schneggenburger R, Neher E (2002) Estimation of quantal parameters at the calyx of Held synapse. *Neuroscience research* 44:343-356.
- Sanes DH (1990) An in vitro analysis of sound localization mechanisms in the gerbil lateral superior olive. *The Journal of neuroscience : the official journal of the Society for Neuroscience* 10:3494-3506.
- Sanes DH, Rubel EW (1988) The ontogeny of inhibition and excitation in the gerbil lateral superior olive. *The Journal of neuroscience : the official journal of the Society for Neuroscience* 8:682-700.
- Sanes DH, Siverls V (1991) Development and specificity of inhibitory terminal arborizations in the central nervous system. *Journal of neurobiology* 22:837-854.
- Sanes DH, Song J, Tyson J (1992) Refinement of dendritic arbors along the tonotopic axis of the gerbil lateral superior olive. *Brain research Developmental brain research* 67:47-55.
- Satzler K, Sohl LF, Bollmann JH, Borst JG, Frotscher M, Sakmann B, Lubke JH (2002) Three-dimensional reconstruction of a calyx of Held and its postsynaptic principal neuron in the medial nucleus of the trapezoid body. *The Journal of neuroscience : the official journal of the Society for Neuroscience* 22:10567-10579.
- Scheuss V, Schneggenburger R, Neher E (2002) Separation of presynaptic and postsynaptic contributions to depression by covariance analysis of successive EPSCs at the calyx of Held synapse. *The Journal of neuroscience : the official journal of the Society for Neuroscience* 22:728-739.
- Schneggenburger R, Meyer AC, Neher E (1999) Released fraction and total size of a pool of immediately available transmitter quanta at a calyx synapse. *Neuron* 23:399-409.

- Schofield BR, Cant NB (1997) Ventral nucleus of the lateral lemniscus in guinea pigs: cytoarchitecture and inputs from the cochlear nucleus. *Journal of Comparative Neurology* 379:363-385.
- Scott LL, Mathews PJ, Golding NL (2005) Posthearing developmental refinement of temporal processing in principal neurons of the medial superior olive. *The Journal of neuroscience : the official journal of the Society for Neuroscience* 25:7887-7895.
- Smith PH, Joris PX, Yin TC (1993) Projections of physiologically characterized spherical bushy cell axons from the cochlear nucleus of the cat: evidence for delay lines to the medial superior olive. *The Journal of comparative neurology* 331:245-260.
- Smith PH, Joris PX, Yin TC (1998) Anatomy and physiology of principal cells of the medial nucleus of the trapezoid body (MNTB) of the cat. *Journal of neurophysiology* 79:3127-3142.
- Smith PH, Massie A, Joris PX (2005) Acoustic stria: anatomy of physiologically characterized cells and their axonal projection patterns. *Journal of Comparative Neurology* 482:349-371.
- Steinert JR, Postlethwaite M, Jordan MD, Chernova T, Robinson SW, Forsythe ID (2010) NMDAR-mediated EPSCs are maintained and accelerate in time course during maturation of mouse and rat auditory brainstem in vitro. *The Journal of physiology* 588:447-463.
- Sterenborg JC, Pilati N, Sheridan CJ, Uchitel OD, Forsythe ID, Barnes-Davies M (2010) Lateral olivocochlear (LOC) neurons of the mouse LSO receive excitatory and inhibitory synaptic inputs with slower kinetics than LSO principal neurons. *Hearing research* 270:119-126.
- Taschenberger H, von Gersdorff H (2000) Fine-Tuning an Auditory Synapse for Speed and Fidelity: Developmental Changes in Presynaptic Waveform, EPSC Kinetics, and Synaptic Plasticity. *The Journal of Neuroscience* 20:9162-9173.
- Taschenberger H, Leao RM, Rowland KC, Spirou GA, von Gersdorff H (2002) Optimizing synaptic architecture and efficiency for high-frequency transmission. *Neuron* 36:1127-1143.
- Tollin DJ (2003) The lateral superior olive: a functional role in sound source localization. *The Neuroscientist : a review journal bringing neurobiology, neurology and psychiatry* 9:127-143.
- Tuna M, Machado AS, Calin GA (2016) Genetic and epigenetic alterations of microRNAs and implications for human cancers and other diseases. *Genes, Chromosomes and Cancer* 55:193-214.
- von Bekesy G (1956) SIMPLIFIED MODEL TO DEMONSTRATE THE ENERGY FLOW AND FORMATION OF TRAVELING WAVES SIMILAR TO THOSE FOUND IN THE COCHLEA. *Proceedings of the National Academy of Sciences of the United States of America* 42:930-944.
- von Hehn CA, Bhattacharjee A, Kaczmarek LK (2004) Loss of Kv3.1 tonotopicity and alterations in cAMP response element-binding protein signaling in central auditory neurons of hearing impaired mice. *The Journal of neuroscience : the official journal of the Society for Neuroscience* 24:1936-1940.
- Walcher J, Hassfurth B, Grothe B, Koch U (2011) Comparative posthearing development of inhibitory inputs to the lateral superior olive in gerbils and mice. *Journal of neurophysiology* 106:1443-1453.
- Wang LY, Neher E, Taschenberger H (2008) Synaptic vesicles in mature calyx of Held synapses sense higher nanodomain calcium concentrations during action potential-evoked glutamate release. *The Journal of neuroscience : the official journal of the Society for Neuroscience* 28:14450-14458.

- Warr WB (1992) Organization of Olivocochlear Efferent Systems in Mammals. In: The Mammalian Auditory Pathway: Neuroanatomy (Webster DB, Popper AN, Fay RR, eds), pp 410-448. New York, NY: Springer New York.
- Weber, Felmy, Nothwang (2015) Comparative analysis of inhibitory inputs to the superior olivary complex in low- frequency hearing gerbils, high-frequency hearing mice, and congenital deaf mice. In. unpublished.
- Weisz CJ, Rubio ME, Givens RS, Kandler K (2016) Excitation by Axon Terminal GABA Spillover in a Sound Localization Circuit. *The Journal of neuroscience : the official journal of the Society for Neuroscience* 36:911-925.
- Werthat F, Alexandrova O, Grothe B, Koch U (2008) Experience-dependent refinement of the inhibitory axons projecting to the medial superior olive. *Dev Neurobiol* 68:1454-1462.
- Wilcox ER, Burton QL, Naz S, Riazuddin S, Smith TN, Ploplis B, Belyantseva I, Ben-Yosef T, Liburd NA, Morell RJ, Kachar B, Wu DK, Griffith AJ, Riazuddin S, Friedman TB (2001) Mutations in the Gene Encoding Tight Junction Claudin-14 Cause Autosomal Recessive Deafness DFNB29. *Cell* 104:165-172.
- Willaredt MA, Schluter T, Nothwang HG (2015) The gene regulatory networks underlying formation of the auditory hindbrain. *Cellular and molecular life sciences : CMLS* 72:519-535.
- Wimmer VC, Horstmann H, Groh A, Kuner T (2006) Donut-like topology of synaptic vesicles with a central cluster of mitochondria wrapped into membrane protrusions: a novel structure-function module of the adult calyx of Held. *The Journal of neuroscience : the official journal of the Society for Neuroscience* 26:109-116.
- Winter J, Jung S, Keller S, Gregory RI, Diederichs S (2009) Many roads to maturity: microRNA biogenesis pathways and their regulation. *Nature cell biology* 11:228-234.
- Yang YM, Wang LY (2006) Amplitude and kinetics of action potential-evoked Ca²⁺ current and its efficacy in triggering transmitter release at the developing calyx of Held synapse. *The Journal of neuroscience : the official journal of the Society for Neuroscience* 26:5698-5708.
- Yasunaga S, Grati M, Cohen-Salmon M, El-Amraoui A, Mustapha M, Salem N, El-Zir E, Loiselet J, Petit C (1999) A mutation in OTOF, encoding otoferlin, a FER-1-like protein, causes DFNB9, a nonsyndromic form of deafness. *Nature genetics* 21:363-369.
- Yorgason JG, Fayad JN, Kalinec F (2006) Understanding drug ototoxicity: molecular insights for prevention and clinical management. *Expert opinion on drug safety* 5:383-399.
- Youssoufian M, Oleskevich S, Walmsley B (2005) Development of a robust central auditory synapse in congenital deafness. *Journal of neurophysiology* 94:3168-3180.
- Youssoufian M, Couchman K, Shivdasani MN, Paolini AG, Walmsley B (2008) Maturation of auditory brainstem projections and calyces in the congenitally deaf (dn/dn) mouse. *The Journal of comparative neurology* 506:442-451.
- Zhang H, Kelly JB (2006) Responses of Neurons in the Rat's Ventral Nucleus of the Lateral Lemniscus to Monaural and Binaural Tone Bursts. *Journal of neurophysiology* 95:2501-2512.
- Zheng QY, Johnson, K.R., Erway, L.C. (1999) Assessment of hearing in 80 inbred strains of mice by ABR threshold analyses. *Hearing research*.

LIST OF ABBREVIATIONS

AMPA	α -amino-3-hydroxy-5-methyl-4-isoxazolepropionic acid
AVCN	Anteroventral cochlear nucleus
DCN	Dorsal cochlear nucleus
ENU	N-ethyl-N-nitrosourea
EPSC	Excitatory postsynaptic current
GBCs	Globular bushy cells
IC	Inferior colliculus
IHCs	Inner hair cells
ILD	Interaural level differences
ITD	Interaural time differences
IPSC	Inhibitory postsynaptic current
LSO	Lateral superior olive
mEPSC	Miniature EPSC
mIPSC	Miniature IPSC
miRNA	microRNA
mRNA	Messenger RNA
MNTB	Medial nucleus of the trapezoid body
MSO	Medial superior olive
NMDA	N-Methyl-D-aspartate
OHCs	Outer hair cells
PVCN	Posterior ventral cochlear nucleus
RISC	RNA-induced silencing complex
RNA	Ribonucleic acid
SBCs	Spherical bushy cells
SOC	Superior olivary complex
TJ	Thigh junction
VCN	Ventral cochlear nucleus
VNLL	Ventral nucleus of the lateral lemniscus

LIST OF FIGURES

Figure 1: Schematic drawing of the mammalian auditory brainstem.....	16
Figure 2: mIPSCs in the developing LSO of mice and gerbils.....	43
Figure 3: evoked IPSCs in pre-hearing mice and gerbils.....	46
Figure 4: Passive properties of LSO neurons.....	50
Figure 5: Firing patterns and action potentials in LSO neurons.....	52
Figure 6: Miniature inhibitory and excitatory events in the LSO.....	54
Figure 7: Evoked excitatory and inhibitory postsynaptic currents in LSO neurons.....	55
Figure 8: Pre- and postsynaptic morphology in the MNTB.....	60
Figure 9: Passive membrane properties of MNTB neurons.....	62
Figure 10: Firing behavior of MNTB neurons.....	66
Figure 11: Action potential properties.....	68
Figure 12: Miniature EPSCs in the MNTB.....	70
Figure 13: Characterization of large and small inputs.....	73
Figure 14: Cumulative EPSCs.....	76
Figure 15: Characterization of AMPA and NMDA currents.....	78

DANKSAGUNG

Von allen, die zum Gelingen dieser Arbeit und zum nötigen Spaß drum herum beigetragen haben, möchte ich mich als erstes bei Felix Felmy bedanken. Danke für Deine ansteckende Begeisterung, Deine Geduld und die tolle Unterstützung sogar noch von Hannover aus! Eine bessere Betreuung hätte ich mir nicht wünschen können!

Ich möchte mich auch besonders bei Benedikt Grothe bedanken für seine Unterstützung, seinen hilfreichen Input zu meiner Arbeit und dafür, dass ich in meiner Zeit in der Neurobiologie so viel lernen konnte, auch über mein Thema hinaus.

Ich bedanke mich außerdem bei Hans Gerd Nothwang und Tina Schlüter aus Oldenburg für die produktive und gute Zusammenarbeit!

Ich danke auch allen anderen die dazu beigetragen haben, dass die letzten Jahre erfolgreich, lehrreich und lustig waren und mir immer in guter Erinnerung bleiben werden. Danke an meine Arbeitsgruppe und speziell an meinen immer hilfsbereiten Zimmerkollegen Julian. Ein besonderer Dank auch an Dani und Steffi für die gute Zeit in der Arbeit und außerhalb, für viel Spaß und Hilfe, euren Input zu meiner Doktorarbeit und für noch so viel mehr! Danke auch an Hilde, Olga und Bea, die mir bei unzähligen Gelegenheiten im Labor geholfen haben und immer ein offenes Ohr, einen guten Rat oder ein paar Süßigkeiten für mich übrig hatten! Vielen Dank auch an Moni und besonders an Sabrina, nicht nur für ihre tolle Arbeit im Tierstall sondern auch für viele nette Gespräche. Danke an alle, die die Neurobiologie zu so einem produktiven und netten Ort zum Arbeiten gemacht haben, für viel gegenseitige Hilfe und Unterstützung, für Pizza, Bier, Fußball spielen und „awesome dinners“!

Zum Schluss möchte ich mich noch bei meiner Familie und meinen Freunden für ihre Unterstützung bedanken, besonders bei Daniel, Karin und Bene fürs Korrekturlesen und ihre Kommentare. Bene, du hast mich während des Schreibens mit allem versorgt was ich mir wünschen konnte (Computer, Kuchen, Motivation...) und ich kann dir gar nicht genug für deine unendliche Geduld und Hilfe danken!